Development of Energy Down Conversion (Quantum cutting) Materials

Adiya Yersin, B. Sc. In Chemical Technology

Submitted in fulfillment of the requirements for the degree of Master of Science in Chemical and Materials Engineering

School of Engineering and Digital Sciences

Department of Chemical and Materials Engineering

Nazarbayev University

53 Kabanbay Batyr Avenue,

Astana, Kazakhstan, 010000

Supervisors: Chang-Keun Lim

April 2023

DECLARATION

I hereby, declare that this manuscript, entitled “Development of Energy Down Conversion (Quantum cutting) Materials”, is the result of my own work except for quotations and citations which have been duly acknowledged.

I also declare that, to the best of my knowledge and belief, it has not been previously or concurrently submitted, in whole or in part, for any other degree or diploma at Nazarbayev University or any other national or international institution.

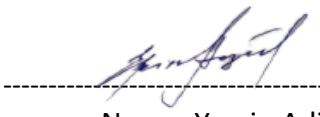

Name: Yersin Adiya

Date: 04.05.2023

Acknowledgements

I would like to express my sincere gratitude to the following individuals who have played an instrumental role in the completion of my master's thesis:

First and foremost, I would like to express my deepest appreciation to my thesis advisor, Professor Chang-Keun Lim. His unwavering guidance, support, and valuable insights throughout the research process have been instrumental in shaping this work. His mentorship has been invaluable, and I am truly grateful for the opportunity to work with such a distinguished scholar.

I would also like to extend my gratitude to Seiilgazy Maira, a research assistant who has been an invaluable member of my research team. Her technical support, research assistance, and willingness to help have been an asset to the success of this project.

Finally, I would like to express my heartfelt thanks to Yerkin Shabdan for his invaluable assistance in the research process. His contribution has been highly appreciated and has been instrumental in achieving the goals of this thesis.

I am also grateful to my family and friends for their constant support and encouragement throughout this journey. Their love and support have given me the motivation to persevere and complete this thesis.

Once again, thank you to all who have contributed to this work. Your support and encouragement have been greatly appreciated.

Abstract

This research aims to develop lanthanide-based metal-organic frameworks (MOFs) with aggregation-induced emission (AIE) ligands to achieve direct sensitization from the ligand to the lanthanide ion. AIE ligands composed of AIE active cores and multiple carboxylic acid groups form a contiguous structure with Ln ions and AIE luminophores to obtain direct sensitization in zero-distance. The quantum cutting (QC) process is considered using Tb^{3+} as the sensitizer ion and Yb^{3+} as the activator ion. A solid-fluorescent ligand, dihydroxyterephthalic acid (DHTA), is used to improve UV light absorption and transfer energy via coordination bonds to solve the concentration quenching issue that reduces quantum cutting efficiency. The energy conversion efficiency of the prepared MOFs is evaluated using intensive optical measurements. This study is novel as it employs AIE or low concentration quenching fluorescent ligands, which is different from the conventional fluorescent ligands for Ln-MOF, and addresses the concentration quenching issue. The research contributes to the development of energy downconversion materials made of lanthanide metal-organic frameworks with AIE ligands, with potential applications in solar energy conversion. The results of photoluminescence (PL) spectroscopy analysis of Ln-AIE MOFs with the DHTA and TPA ligands at different Tb concentrations (8%, 12%, and 15%) show that the AIE ligand sensitization is successfully demonstrated. The emission peaks of Yb^{3+} in the near-infrared range correspond to the transitions $^2F_{5/2} \rightarrow {}^2F_{7/2}$ as a result of QC. Quantum resonance energy transfer from Tb^{3+} to Yb^{3+} is observed only when the AIE ligand is incorporated in the MOF structure, which is a characteristic of quantum cutting. The AIE ligand sensitized Ln-MOF have a strong potential to improve solar energy conversion efficiency of single hetero-junction solar cell.

Keywords: Quantum cutting, Downconversion, Aggregation Induced Emission (AIE), Metal Organic Frameworks (MOF), Lanthanides, Ligands, Solar cell

Table of contents

List of Abbreviation & Symbols

Ln	Lanthanide
MOF	Metal Organic Frameworks
AIE	An Aggregation-Induced Emission
DC	Down Conversion
QC	Quantum cutting
CQ	Concentration quenching
DHTA	2,5-dihydroxyterephthalic acid
TPA	Terephthalic acid
TMA	Trimesic acid

List of Figures

Chapter 1- Introduction

The objective of the work

The dye-sensitization strategy for down-conversion nanoparticles, reinforcing the poor light-absorption property of lanthanide (Ln) nanophosphors, has strong potential to realize the energy transformation of solar light. Even though the strategy was optimized by aggregation-induced emission (AIE) sensitizers, still, the strategy is limited by the fluorescence resonance energy transfer (FRET) radius. The objective of this work is to synthesize Ln-based metal-organic frameworks (MOFs) using AIE (aggregation-induced emission) ligands as the matrix hosting for the Ln ions in order to achieve direct sensitization from the ligand to the Ln in zero-distance (Figure 1.1). The AIE ligands used in this study will be composed of AIE active core and multiple carboxylic acid groups, which will form a contiguous structure composed of Ln ions and AIE ligands for direct sensitization. The variation of ligand will be used to tune the distance between the sensitizer/activator ions pair. The QC (quantum cutting) process will be considered, using Tb^{3+} as the sensitizer ion and Yb^{3+} as the activator ion. The energy conversion efficiency of the prepared MOFs will be evaluated using intensive optical measurements, and the achieved MOFs will be demonstrated to improve the solar cell efficiency.

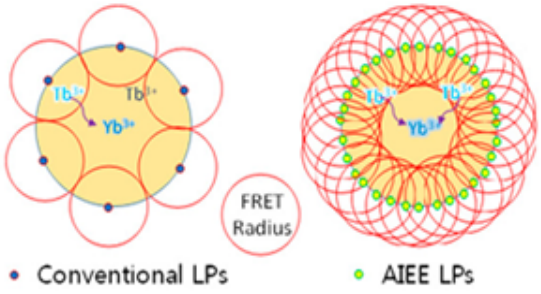

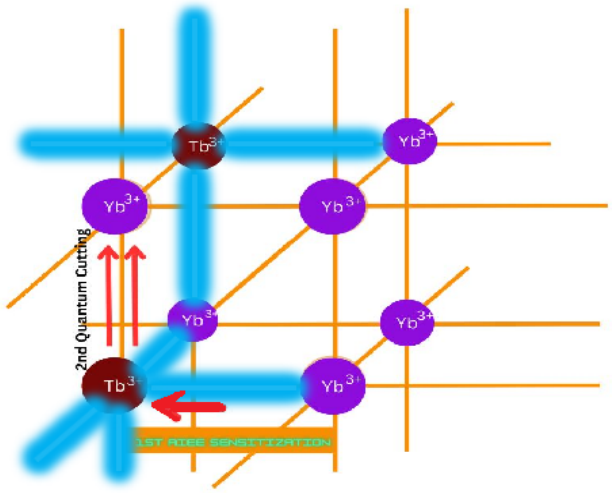

Figure 1.1. The concept of QC from Ln-AIE MOF

The novelty of the research

The originality of this work lies in the internal sensitization of down-conversion by the use of AIE or low concentration quenching fluorescent ligands in Ln-MOF. We incorporate dihydroxyterephthalic acid (DHTA) an the non-concentration quenching ligand. If we utilize a conventional fluorescent ligands for Ln-MOF, the concentration quenching issue will prohibit an efficient down-conversion (quantum cutting (QC)). The AIE ligand sensitized Ln-MOF have a strong potential to improve solar energy conversion efficiency of single hetero-junction solar cell.

The Aim of the work.

The main aim of this work is the Development of Energy Downconversion (Quantum Cutting) Materials Made of Lanthanide Metal-Organic Frameworks with AIE ligands.

Chapter 2- Literature Review

Currently, a renewable energy source is solar energy. This has minimal adverse effects on the environment. Solar energy is anticipated to supply 16% of the world's electricity in the future. [1]. What is the ideal response to the energy crisis? Numerous researches have been conducted in the recent years with a focus on the efficient use of solar energy. Studies have often been done in two ways to maximize efficiency. 1. based on the quest for novel substances or techniques. which efficiently investigates the photovoltaic effect. 2. The solar spectrum has changed to make it compatible with the solar cell's spectrum efficiency. New materials were investigated in the first instance. Thin-film technology, organic solar cells, and their possible future applications are all taken into account. [2], [3].

Quantum dots were used to illustrate a method of producing multiple excitons, which was predicted to boost internal efficiency by more than 100% [4]. The efficiency of solar cells can also be increased using alternative techniques such texturing silicon solar cells, using scattering particles, and improving the manufacturing process [5]. Another strategy employs a different setup with many transitions for efficient solar spectrum analysis [6]. On the other hand, a solar cell's degradation from exposure to ultraviolet light is a significant risk factor that lowers its efficiency. With an efficiency of roughly 18%, crystalline silicon (c-Si) solar cells dominate the commercial photovoltaic energy markets. [7]. The c-Si band gap, which theoretically has a greatest scale of 30%, and the so-called spectral conflict with the solar spectrum prevent the current efficiency from being comparable to the Shockley-Queisser limit. [7]. Due to electron recombination and thermal

relaxation, photons in the ultraviolet and visible (UV-visible) ranges with energy above thermal are lost in the band gap, while photons with energy below the band gap are not absorbed. (Figure. 2.1) A significant increase in conversion efficiency is expected if this region of the input spectrum can be tuned to a wavelength in the c-Si absorption range. [8]

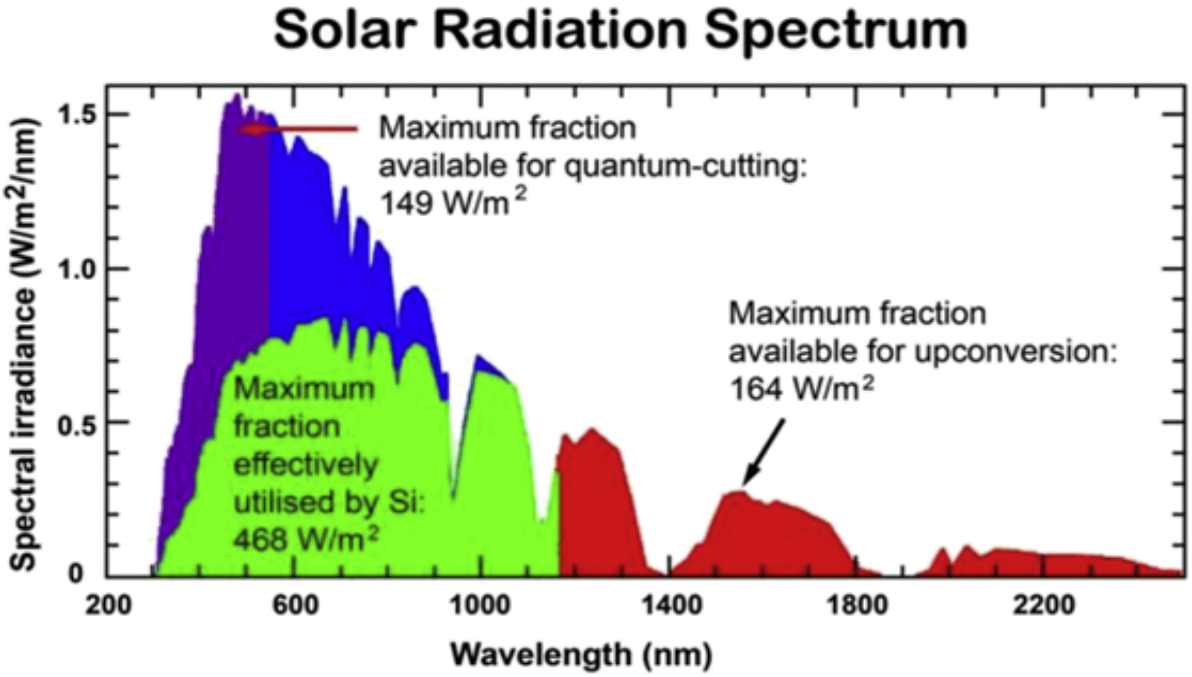

Figure 1. Solar Radiation Spectrum. [9]

The band gap of solar cells and the imbalance with the sun spectrum are the main contributors to the low efficiency of photovoltaic conversion [10]. In other words, photons whose energies are below the band gap cannot be absorbed, whereas photons whose energies are beyond the band gap thermalize hot charge carriers and release extra energy [11]. In this situation, it is possible to manipulate the solar spectrum using the step-down and step-up conversion processes in photonic materials, particularly in those doped with rare earth element ions [12]. Quantum cutting (down conversion) is a fascinating mechanism that should be researched utilizing materials doped with rare earth elements. High quantum efficiencies can result from the conversion of high energy photons into low energy photons in this process.

2.1 Quantum cutting process

Quantum cutting is a process in which a high-energy photon (usually in the ultraviolet or blue

region of the spectrum) is converted into two or more lower-energy photons (usually in the visible or near-infrared region). This process is of particular interest for applications in photovoltaics, solid-state lighting, and biological imaging. This process is illustrated using two types of ions, ion 1 and ion 2, with hypothetical energy-level schemes as shown in Figure 2.2.

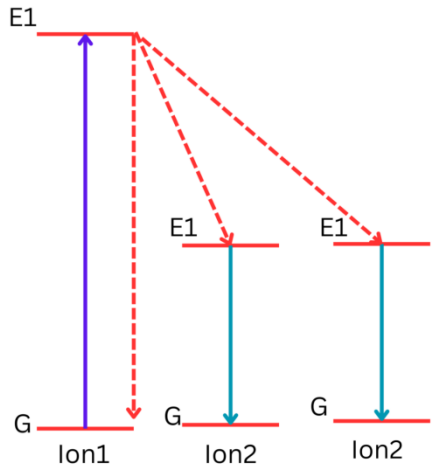

Figure 2.2 Quantum cutting process

Ion 1 ions can emit from a high-energy level, while ion 2 ions undergo energy transfer. In the case of NIR quantum cutting applied to solar cells, the ion 2 should always be focused on the Yb^{3+} ion, and the ion 1, as a donor, must be matched with Yb^{3+}. Specifically, there should be an energy level with twice the energy difference to the $^2F_{5/2}$-$^2F_{7/2}$ transition of Yb^{3+}. There are two types of donor, one with and the other without an intermediate level at around 10,000 per cm, in accordance with first-order and second-order energy transfer, respectively. Based on the Dieke Diagram evaluation, potential donors for this process include Pr^{3+}, Nd^{3+}, Ho^{3+}, Er^{3+}, Tb^{3+}, and Tm^{3+} ions. The first four have an intermediate level, while the latter two do not, as shown in Figure 2.3 [13]

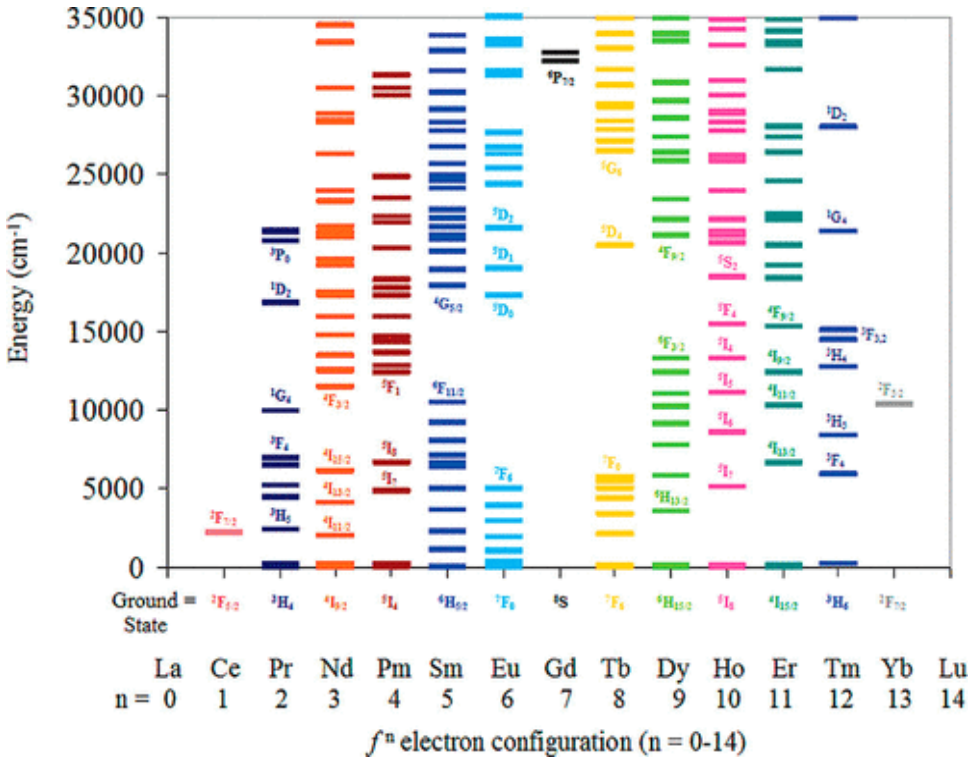

Figure. 2.3. Dieke diagram showing the energy level structure of rare-earth ions from Ce^{3+} to Yb^{3+} [14]

One example of quantum cutting involves the use of rare earth ions (such as europium or terbium) embedded in a host material. When a high-energy photon is absorbed by the rare earth ion, it undergoes a non-radiative transition to a higher energy state. This higher energy state is then rapidly de-excited through a series of non-radiative transitions until it reaches a lower energy state. At this point, the rare earth ion can emit two or more lower-energy photons, each with a wavelength longer than that of the original photon.

Quantum cutting can increase the efficiency of solar cells by converting high-energy photons into lower-energy photons that are more easily absorbed by the semiconductor material. It can also increase the efficiency of solid-state lighting by converting ultraviolet or blue light into visible light. On the other hand, QC needs a high energy excitation, which has short penetration length and high toxicity.

Dopants and Host materials for QC process.

Dopants and host materials are needed for quantum cutting (QC) process to achieve efficient down-conversion of high-energy photons.

Dopants are impurities that are introduced into a host material in order to modify its optical or electronic properties. In the context of quantum cutting, dopants are selected based on their ability to absorb high-energy photons and transfer the absorbed energy to the host material, which then emits multiple low-energy photons. Common dopants for quantum cutting applications include rare earth ions (such as Eu^{2+} and Tb^{3+}) and transition metal ions (such as Cr^{3+}).

The host material is the primary material in which the dopants are embedded. In the context of quantum cutting, the host material should have a wide bandgap to minimize energy losses due to non-radiative recombination. Selecting appropriate host materials for quantum computing requires materials with low phonon energy to prevent undesirable multiphonon relaxation processes, which may interfere with the QC process. Luminescent carriers, such as fluoride (~355 per cm), iodides (~144 per cm), bromide (~172 per cm), and chloride (~260 per cm), are considered ideal for this purpose.[14] Nevertheless, due to their hygroscopic nature, chlorides, bromides, and iodides have limited use, and therefore, fluoride is the most preferred carrier due to its high stability and low phonon energy, providing the best of both worlds. Common host materials for quantum cutting applications include silica, alumina, and other glasses and ceramics.[15]

The selection of dopants and host materials for quantum cutting applications involves several factors. In addition to the bandgap and absorption cross-section discussed earlier, dopants should also have a relatively long excited state lifetime to allow for efficient energy transfer to the host material. The energy level alignment between the dopant and host material is also important, as it determines the efficiency of energy transfer between them.

Other factors that can influence the selection of dopants and host materials for quantum cutting applications include the desired emission wavelength, luminescence quantum yield, and thermal stability. For example, some dopants may emit at longer wavelengths than others, which can affect

the suitability of the host material. Similarly, some dopants may have higher luminescence quantum yields or better thermal stability, which can make them more desirable for certain applications.

Overall, the selection of dopants and host materials for quantum cutting applications requires a careful consideration of all of these factors, in order to achieve the desired performance characteristics.

2.2 Lanthanide doped nanophosphors

Lanthanide (Ln)-doped nanophosphors have also been explored for use in quantum cutting applications. The quantum cutting efficiency of these nanophosphors can be enhanced by reducing the size of the particles, which can result in increased absorption and emission of light. Additionally, the use of Ln-doped nanophosphors can provide advantages over conventional luminophores, such as improved stability, lower toxicity, and tunable emission wavelengths.

Several studies have reported on the use of Ln-doped nanophosphors for quantum cutting. For example, one study investigated the use of Eu^{3+} and Yb^{3+} co-doped nanophosphors for quantum cutting in solar cells. The study found that the nanophosphors exhibited efficient quantum cutting and enhanced the overall efficiency of the solar cell. [16]. Another study explored the use of Ce^{3+} and Yb^{3+} co-doped nanophosphors for quantum cutting in LEDs, demonstrating improved efficiency compared to conventional luminophores.[17]

Limitations of Lanthanide doped nanophosphors

One limitation of lanthanoids is their susceptibility to environmental interference, such as magnetic fields, temperature changes, and radiation. These factors can cause decoherence in the quantum states of the lanthanoid ions, leading to errors in calculations. To mitigate this, lanthanoid-based QC systems often require sophisticated isolation and shielding techniques to protect them from external interference.

Another limitation of lanthanoids in QC processes is their complex energy level structure. Lanthanoids have multiple electronic states that can interact with each other, leading to decoherence and errors in calculations. This complexity also makes it challenging to manipulate the electronic states of the lanthanoid ions, which is crucial for performing quantum operations.

Furthermore, lanthanoid-based QC systems are typically more challenging to fabricate and operate than other types of quantum systems, such as superconducting qubits or ion traps. This is because the lanthanoid ions are often embedded in solid-state matrices, requiring specialized fabrication techniques and equipment.

2.3 Concentration quenching

Concentration quenching is a phenomenon that occurs in luminescent materials, such as phosphors or quantum dots, where the luminescence intensity decreases as the concentration of the luminescent material increases.

This occurs due to the presence of non-radiative energy transfer pathways between the luminescent species, where the excited state energy is transferred to a neighboring molecule without emitting a photon. This non-radiative energy transfer becomes more significant at higher concentrations of luminescent material, leading to a decrease in luminescence intensity with increasing concentration.

Concentration quenching is an important consideration when designing and optimizing luminescent materials for various applications, as it limits the maximum concentration of luminescent material that can be used without significant reduction in luminescence efficiency. To mitigate concentration quenching, various strategies can be employed, such as optimizing the distance between luminescent species or using core-shell structures that separate the luminescent species from each other.

2.4 Aggregation-induced emission

High concentrations frequently diminish or quench luminescence, a phenomenon known as "concentration quenching." The concentration quenching effect has probably been referred to as "aggregation-caused quenching (ACQ)" since one of the key causes of the quenching process is mechanistically linked to the "formation of aggregates" . [18]. The term "aggregation-induced emission" (AIE) refers to a photophysical phenomenon associated with chromophore aggregation and was first used by Tang et al. in 2001 [19]. Due to the nonradiative decay of their excited states caused by intramolecular movements, AIE molecules are practically non-emissive in diluted solutions, yet they typically exhibit spectacular solid-state emission. [20]

As opposed to conventional luminophores, which suffer from significant emission quenching,

aggregation-induced emission (AIE) fluorophores exhibit significantly enhanced fluorescence in aggregated states, making them the ideal materials for laser fabrication to create highly fluorescent nanoparticles. [21] There are a number of strategies that could be used to counteract the concentration quenching characteristic of AIE luminophores (LPs), including:

- Rotational relaxation, such as that found in tetraphenylethene, can limit the dissipation of nonradiative energy;[21]
- Extending p-conjugation from twisted conformations by inducing planarization (e.g., bis-(styryl) anthracene derivatives);[22]
- Head-to-tail arrangement of the transition dipole moment (J-aggregation), for example, in derivatives of the compound cyanostilbene;[23]
- preventing solvent molecules (such as hydroxyphenyl benzoxazole) from interacting with intramolecular hydrogen bonds when they are gathered together. [23]

Diethyl 2,5-dihydroxyterephthalate (DT) is another name for dihydroxyterephthalic acid (DHTA). Due to its high fluorescence efficiency (FLY = 0.71 in THF and 0.45 in water suspension of nanoaggregates) even in the solid state, diethyl 2,5-dihydroxyterephthalate (DT) was chosen as a fluorescent unit. This made it appropriate for making dye concentrated nanoprobes. By bis-sulfonylating the parent dye (DT), pentafluorophenylsulfonyl (pFS) group 13–14 significantly reduced the fluorescence of the parent dye (DT). It is displayed in figure 2.5. [24]

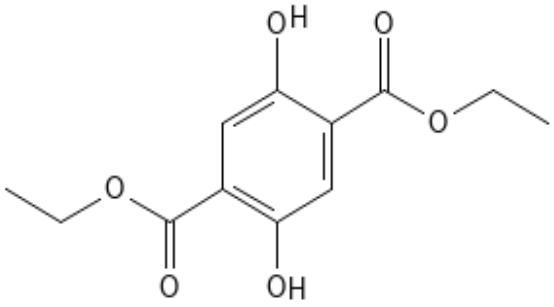

Figure. 2.5. 2,5-dihydroxyterephthalic acid (DHTA) structural formula.

Another article uses DHTA with Ln^{3+} ions that is shown in this case.In this case, the article mentioned is exploring the use of DHTA (dihydroxyterephthalic acid) with Ln3+ ions (lanthanide ions) to enhance the quantum cutting efficiency of the nanophosphors. Specifically, they looked

at Tb^{3+}/Yb^{3+} nanoparticles (NPs) doped with DHTA.[25]

The researchers found that after sensitization (a process where a sensitizer is used to increase the efficiency of energy transfer from one molecule to another), there was a significant increase in absorbance in the ultraviolet region and photoluminescence (PL) at 980 nm. This means that the nanoparticles were able to absorb more light in the ultraviolet region and emit light at a longer wavelength (980 nm), which is useful for applications such as solar cells and LEDs.This study suggests that using DHTA with Ln^{3+} ions can be an effective way to enhance the quantum cutting efficiency of nanophosphors.[25]

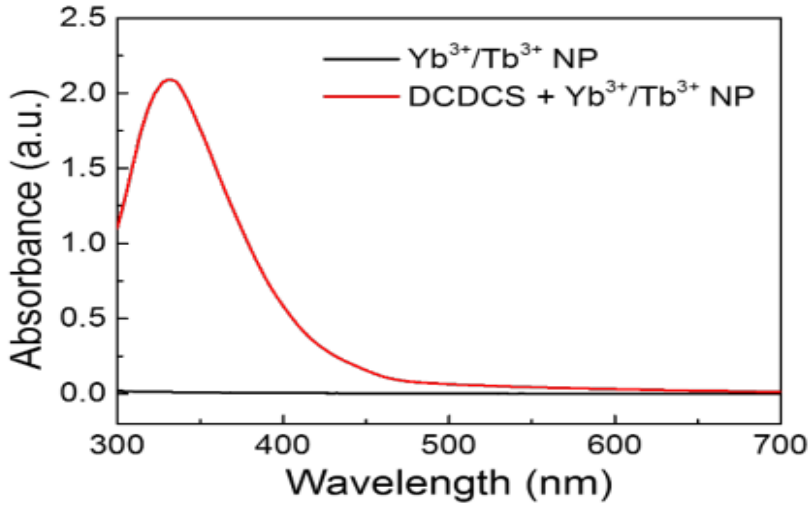

Figure 2.6. Absorbance spectra of $NaYF_4$:50%Yb^{3+},12%Tb^{3+} NP suspension with (red) or without (black) AIE. Wei Shao et al. [25]

Also, Dihydroxyterephthalic acid (DHTA) is a commonly used ligand in the synthesis of Metal-Organic Frameworks (MOFs), which are a class of porous materials made of metal ions or clusters connected by organic ligands. DHTA contains two hydroxyl (-OH) groups and two carboxylic acid (-COOH) groups, which can form strong coordination bonds with metal ions to create stable MOF structures.

There are several reasons why DHTA is a popular choice as a ligand in MOF synthesis:

- Strong Coordination Ability: DHTA has four binding sites that can form strong coordination bonds with metal ions, resulting in stable and robust MOF structures.[26]
- Control Over Pore Size: The size of the pores in a MOF can be controlled by adjusting the

length of the ligand used. DHTA is a relatively long ligand, which can result in larger pores in the MOF structure.[27]

- Hydrophilic Nature: The presence of the hydroxyl (-OH) groups in DHTA can make the MOF structure more hydrophilic, which can enhance its stability and solubility in aqueous environments.[28]

Overall, DHTA's strong coordination ability, control over pore size, hydrophilic nature, and biocompatibility make it a versatile and popular ligand in the synthesis of MOFs with a range of applications in fields such as catalysis, gas storage, and sensing.

Elimination of the limitation of lanthanides in quantum cutting using organic dye AIE

An organic dye with AIE (aggregation-induced emission) properties could potentially be used in combination with lanthanides to address some of the limitations of lanthanides in quantum cutting. AIE dyes are a class of materials that exhibit enhanced emission when they are aggregated or confined, making them useful for a variety of applications, including sensing, imaging, and optoelectronics.

AIE (Aggregation-Induced Emission) dyes are important because they can enhance the efficiency of quantum cutting by increasing the photon absorption and energy transfer processes within the MOF. The AIE effect occurs when a dye molecule is in a dispersed state, resulting in weak fluorescence, but when the molecule aggregates, its fluorescence is enhanced. This is due to the restriction of molecular rotation and vibration caused by the aggregation, which can increase the radiative decay rate and reduce the nonradiative decay rate, resulting in an overall increase in fluorescence efficiency.

In the case of Ln-AIE MOFs, the AIE dyes can act as sensitizers for the lanthanide ions, increasing their absorption of photons and promoting energy transfer to the lanthanide ions for quantum cutting. This can result in higher efficiency and intensity of the emitted photons, making the Ln-AIE MOFs potentially useful for applications

Dye-sensitized up-conversion and dye-sensitized down-conversion concept

Dye-sensitized up-conversion and dye-sensitized down-conversion are two concepts related to the conversion of light from one wavelength to another using dyes. In both cases, the dye acts as a sensitizer to enhance the conversion process.

In Dye-sensitized up-conversion, a dye is used to sensitize the excited state of an up-conversion material . Up-conversion material absorbs two or more photons of low energy (typically in the near-infrared range) and emits a single photon of higher energy (usually in the visible range). The dye is used to absorb light in the visible range and transfer the energy to the excited state of the up-conversion material, increasing the efficiency of the up-conversion process.

In dye-sensitized down-conversion, a dye is used to sensitize the excited state of a down-conversion material. The down-conversion material absorbs a single photon of high energy (typically in the ultraviolet or visible range) and emits two or more photons of lower energy (usually in the visible or near-infrared range). The dye is used to absorb light in the ultraviolet or visible range and transfer the energy to the excited state of the DCM, increasing the efficiency of the down-conversion process.

2.5 Metal Organic Frameworks

Metal-organic frameworks (MOFs) are a class of crystalline materials composed of metal ions or clusters linked by organic ligands. MOFs have garnered significant attention in recent years due to their tunable pore sizes and high surface areas, which make them promising candidates for various applications, including gas storage, separation, sensing, catalysis, and drug delivery.

MOFs were first discovered in the late 1990s and have since become a rapidly growing field of research. One of the main advantages of MOFs is their ability to be designed with precise control over their structures and properties. The unique combination of metal ions or clusters and organic ligands can lead to a vast array of possible structures and properties, making MOFs highly customizable for different applications.

The structure of MOFs is based on the coordination of metal ions or clusters with organic ligands. The metal ions or clusters act as the nodes, and the organic ligands act as the connectors between

them, forming a three-dimensional network. The resulting structure is highly porous, with regular cavities or channels of varying sizes and shapes. Its shown in a figure 2.7

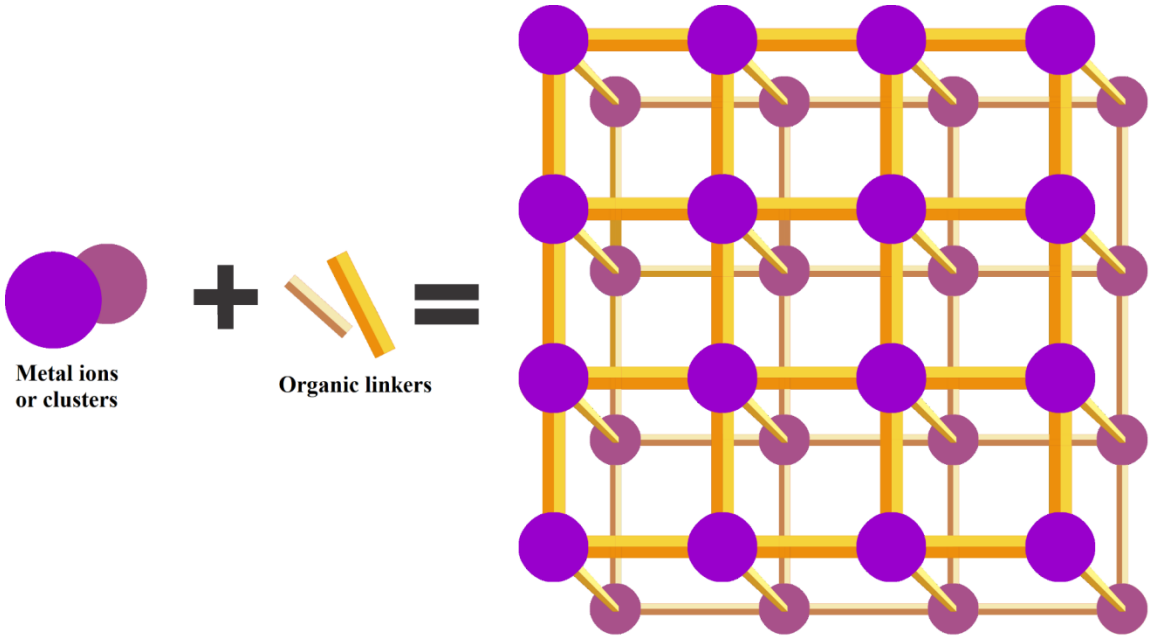

Figure 2. 7. Metal-Organic Framework

One promising application of MOFs is in the field of quantum cutting. Quantum cutting refers to the process of converting high-energy photons into multiple lower-energy photons, which can be harnessed for energy harvesting applications such as solar cells. This process can be achieved through the use of materials that contain lanthanide ions, which have the ability to undergo radiative energy transfer. The use of MOFs as hosts for lanthanide ions offers several advantages over other types of materials. MOFs are highly tunable, allowing for the optimization of the properties of the material for a specific application. The porous nature of MOFs also allows for the incorporation of multiple lanthanide ions, which can further enhance the quantum cutting efficiency. In addition, MOFs are environmentally friendly and easy to prepare, making them attractive for large-scale production. The use of MOFs in quantum cutting also has the potential to address the limitations of current photovoltaic materials, which are limited in their ability to absorb the full spectrum of sunlight.

Another example of the use of MOFs with lanthanide in the development of lanthanide-doped upconversion nanoparticles (UCNPs). UCNPs are capable of converting near-infrared light into

visible light, which can be harnessed for imaging and sensing applications. MOFs can be used as hosts for UCNPs, allowing for the incorporation of multiple lanthanide ions and the optimization of the properties of the material for specific applications.

Overall, the use of MOFs in quantum cutting offers a promising avenue for the development of next-generation photovoltaic materials and other energy harvesting applications. The tunable properties of MOFs, coupled with their ability to act as hosts for lanthanide ions, make them attractive candidates for the development of highly efficient quantum cutting materials. Further research in this area has the potential to lead to significant advances in the field of renewable energy.

Methods for synthesizing MOF

Metal-organic frameworks (MOFs) are a type of crystalline material that consist of metal ions or clusters coordinated to organic ligands. There are several methods for synthesizing MOFs, including:

- Solvothermal Synthesis: This is the most common method used for synthesizing MOFs. It involves heating a mixture of metal salts and organic ligands in a solvent at high temperatures and pressures. The solvent used is typically a polar aprotic solvent like dimethylformamide or dimethylacetamide.
- Hydrothermal Synthesis: This method is similar to solvothermal synthesis but uses water as the solvent. The synthesis is typically carried out in a sealed vessel at high temperature and pressure.
- Microwave-Assisted Synthesis: This method involves heating a mixture of metal salts and organic ligands in a microwave oven. The advantage of this method is that it is faster than traditional heating methods and can lead to the formation of highly crystalline MOFs.
- Mechanochemical Synthesis: This method involves grinding together the metal salts and organic ligands in the presence of a small amount of solvent. This method has the advantage of being a solvent-free method and can lead to the formation of highly crystalline MOFs.
- Electrochemical Synthesis: This method involves the use of an electrochemical cell to synthesize MOFs. The metal ions are reduced at the cathode and react with the organic ligands in the solution to form the MOFs.

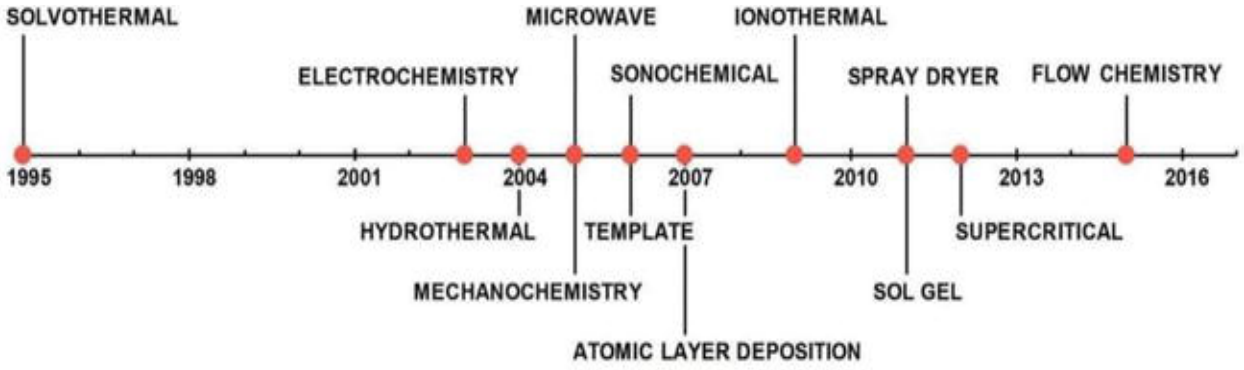

Figure 2.8. Time line of the most common synthesis approaches for MOF [33]

Each of these methods has its advantages and disadvantages, and the choice of method depends on the specific MOF being synthesized and the desired properties of the final material.

Based on these methods, we chose the most promising one for us. This is Solvothermal Synthesis

Chapter 3- Materials and method

Materials

Terbium (III) chloride hexahydrate ($TbCl_3 \cdot 6H_2O$, 99.99%) from Sigma-Aldrich. Ytterbium (III) chloride hexahydrate ($YbCl_3 \cdot 6H_2O$, 99.99%) from Sigma-Aldrich. Yttrium (III) nitrate hexahydrate ($Y(NO_3)_3 \cdot 6H_2O$, 99.99%) from Sigma-Aldrich. 2,5-Dihydroxyterephthalic acid ($C_8H_6O_6$, 98%), Terephthalic acid ($C_6H_4(CO_2H)_2$, 98%), Trimesic acid ($C_6H_3(CO_2H)_3$, 98%)

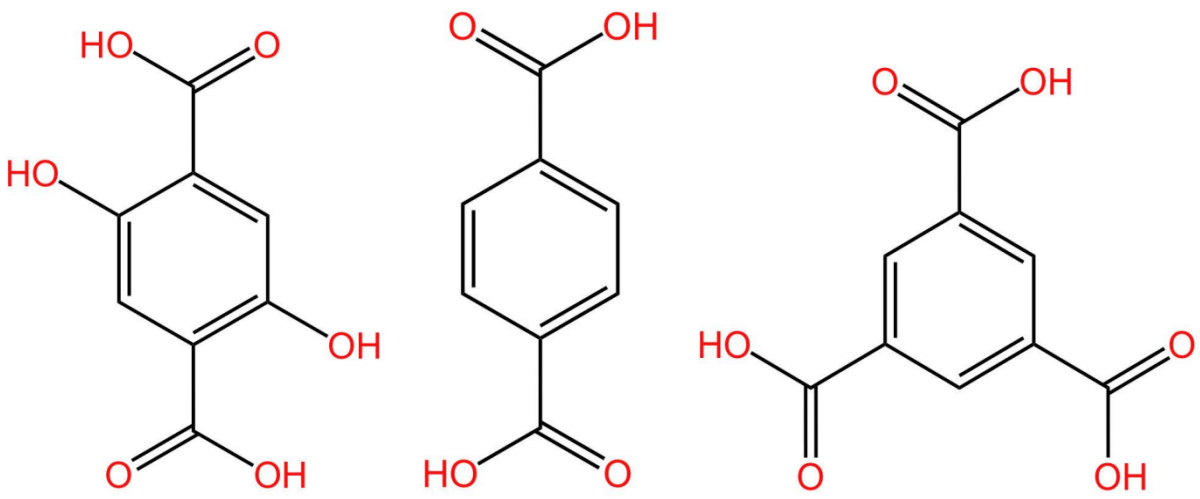

Figure 3.1 Chemical structure of a) 2,5-dihydroxyterephthalic acid (DHTA), b) terephthalic acid (TPA) and c) trimesic acid (TMA)

Characterization

X-ray Diffraction (XRD) System - SmartLab (Rigaku) was used for analyze physical properties (phase composition, crystal structure). X-ray source operated at 40 kV and 50 mA. Nicolet iS10 FT-IR Spectrometer for identify chemical substances. Evolution 300 UV-Vis Spectrophotometer was used for measurments of absorbtion and transmission in the ultraviolet, visble and NIR spectral regions in the wavelength range of 200–1200 nm. To determine a materials thermal stability we used thermograviametric analisis. Photoluminescence Spectrometer (PL) FLS-1000.

Instrumentation

Laboratory Chamber Furnace ELF 1100- Carbolite Gero. Thermo Scientific™ Vacuum Oven.

Chapter 4-Experimental part

Based on an article by Wei Shao et al. [25] on their experimental results, we determined the best concentration of Tb^{3+} ions. Since they are a direct acceptor of energy transfer from the AIEE dye. The best options were 8%, 12% and 15%. And according to these calculations, the further ratio of all reagents was determined.

Calculations

With 12% Tb

$Y_{50\%-x\%}Tb_{x\%}Yb_{50\%}$

This calculation for 1 mmol

$Y(NO_3)_3.6H_2O$	$TbCl_36H_2O$	$YbCl_36H_2O$
0,38 mmol	0,12 mmol	0,5 mmol
145,5 mg	47,7 mg	193,7 mg

This calculation for 0,5 mmol

$Y(NO_3)_3.6H_2O$	$TbCl_36H_2O$	$YbCl_36H_2O$	2,5-Dihydroxyterephthalic
0,19 mmol	0,06 mmol	0,25 mmol	0,5 mmol
73,72 mg	22,43 mg	96,85 mg	99,065 mg

Mass of yield: 174 mg after 158 mg

$Y(NO_3)_3.6H_2O$	$TbCl_36H_2O$	$YbCl_36H_2O$	Terephthalic acid
0,19 mmol	0,06 mmol	0,25 mmol	0,5 mmol
73,72 mg	22,43 mg	96,85 mg	83,65 mg

Mass of yield: 122 mg

With 15% Tb

$Y5_{0\%-x\%}Tb_{x\%}Yb_{50\%}$

This calculation for 1 mmol

$Y(NO_3)_3.6H_2O$	$TbCl_36H_2O$	$YbCl_36H_2O$
0,35 mmol	0,15 mmol	0,5 mmol

134,05 mg	56,07 mg	193,7 mg

This calculation for 0,5 mmol

$Y(NO_3)_3.6H_2O$	$TbCl_36H_2O$	$YbCl_36H_2O$	2,5-Dihydroxyterephthalic
0,175 mmol	0,075 mmol	0,25 mmol	0,5 mmol
67,026 mg	28,035 mg	96,85 mg	99,065 mg

Mass of yield: 173 mg

$Y(NO_3)_3.6H_2O$	$TbCl_36H_2O$	$YbCl_36H_2O$	Terephthalic acid
0,175 mmol	0,075 mmol	0,25 mmol	0,5 mmol
67,026 mg	28,035 mg	96,85 mg	83,65 mg

Mass of yield: 150 mg

With 8% Tb

$Y5_{0\%-x\%}Tb_{x\%}Yb_{50\%}$

This calculation for 1 mmol

$Y(NO_3)_3.6H_2O$	$TbCl_36H_2O$	$YbCl_36H_2O$
0,42 mmol	0,08 mmol	0,5 mmol
160,86 mg	29,9 mg	193,7 mg

This calculation for 0,5 mmol

$Y(NO_3)_3.6H_2O$	$TbCl_36H_2O$	$YbCl_36H_2O$	2,5-Dihydroxyterephthalic
0,21 mmol	0,04 mmol	0,25 mmol	0,5 mmol

$Y(NO_3)_3.6H_2O$	$TbCl_36H_2O$	$YbCl_36H_2O$	2,5-Dihydroxyterephthalic
80,43 mg	14,95 mg	96,85 mg	99,065 mg

Mass of yield: 135 mg

$Y(NO_3)_3.6H_2O$	$TbCl_36H_2O$	$YbCl_36H_2O$	Terephthalic acid
0,21 mmol	0,04 mmol	0,25 mmol	0,5 mmol
80,43 mg	14,95 mg	96,85 mg	83,65 mg

Synthesis by Solvothermal methods:

1st Solvothermal method synthesis

A solid mixture of Ln^{3+} ion and 2,5-dihydroxyterephthalic acid (0.5 mol, 99 mg) was mixed with N,N-dimethylformamide (10 ml) and water (1 ml), stirred for 30 minutes for complete dissolution. After that, it was poured into a container in a pressure vessel and heated to 150 °C for 72 hours. Then it was placed in a vacuum oven for complete drying within 24 hours. As a result, we get a crystalline powder.

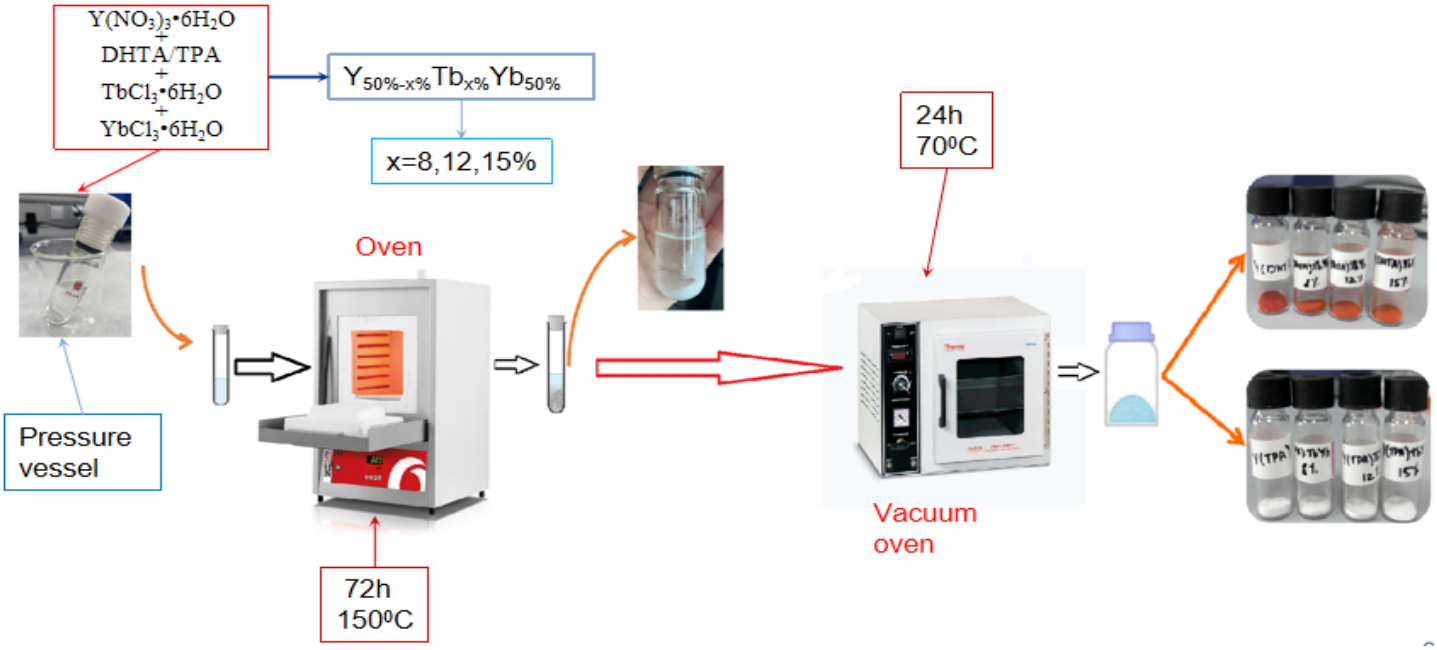

Figure 4.1. Process of Synthesis by Solvothermal method

	Ligand	Tb^{3+} ion concentration	Temperature	Time	Solvent	Color
1	DHTA	8%	150	72h	DMF/H_2O	Bright red
2	DHTA	12%	150	72h	DMF/H_2O	Bright red
3	DHTA	15%	150	72h	DMF/H_2O	Bright red
4	DHTA	12%	110	72h	DMF/H_2O	yellow
5	DHTA	12%	110	100h	DMF	yellow
6	DHTA	12%	120	100h	DMF/H_2O	yellow
7	DHTA	12%	120	24h	DMF/H_2O	red
8	DHTA	12%	85	48h	H_2O/Ethanol	yellow
9	DHTA	12%	85	48h	DMF/H_2O	yellow

	Ligand	Tb^{3+} ion concentration	Temperature	Time	Solvent	Color
1	TPA	8%	150	72h	DMF/H_2O	White
2	TPA	12%	150	72h	DMF/H_2O	White
3	TPA	15%	150	72h	DMF/H_2O	White
3	TPA	12%	120	24h	DMF/H_2O	White

	Ligand	Tb_{3+} ion concentration	Temperature	Time	Solvent	Color
1	TMA	12%	120	24h	DMF/H_2O	White

2nd Solvothermal method synthesis

Also, based on other literature, we decided that combining two ligands would give the better result. Because TMA/TPA can't make good energy transfers. They don't have energy transfer because they also don't have strong emission. In another case DHTA has strong emission, but it's hard to make a good MOF structure. And TMA is a good material for MOF. That's why we mix two ligands.

	Ratio of TMA:DHTA	Tb^{3+} ion concentration	Temperature	Time	Solvent	Color
1	1:1	12%	120	24h	DMF/H_2O	White
2	2:1	12%	120	24h	DMF/H_2O	White
3	4:1	12%	120	24h	DMF/H_2O	White
4	8:1	12%	120	24h	DMF/H_2O	White
5	10:1	12%	120	24h	DMF/H_2O	White

Chapter 5-Results and Discussion

5.1 1st Solvothermal method results

5.1.1 XRD analysis

The X-ray diffraction (XRD) analysis conducted on the newly prepared Ln-AIE MOF samples allowed us to confirm their crystal structures. The first four samples were analyzed, which were prepared with the DHTA ligand at different Tb concentrations (8, 12, 15%) along with a sample of pure Y(DHTA) MOF. The results of the XRD analysis are presented in Figure 5.1.

Based on the XRD patterns, we can observe that all of the samples have sharp and intense peaks, which indicate a highly crystalline structure. The peaks in the XRD patterns of the samples also correspond to the standard reference patterns of the Y(DHTA) MOF, indicating that the samples have a similar crystal structure. The minor differences observed in the peak positions and intensities between the samples can be attributed to the presence of Tb and Yb ions in the MOF, which introduce slight distortions to the crystal structure.

The XRD analysis confirms the successful synthesis of the Ln-AIE MOF samples, and the presence of Tb and Yb ions in the MOF is also confirmed. Additionally, the similarity in the crystal structure between the Ln-AIE MOF samples and the Y(DHTA) MOF indicates that the doping of the MOF with lanthanide ions did not significantly affect the overall crystal structure of the material.

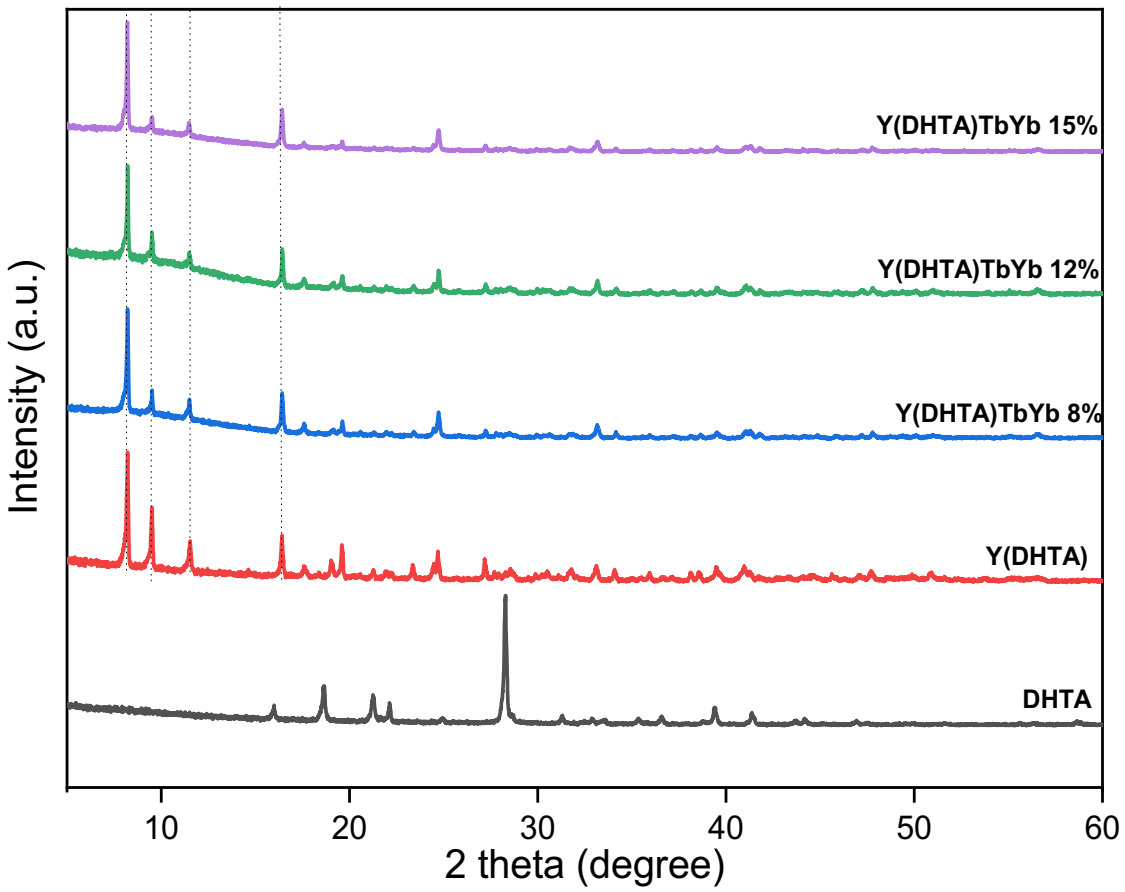

Figure 5.1 X-ray diffraction analysis of Ln-AIE MOFs with the DHTA ligand at different Tb concentrations (8, 12, 15%)

After this, for all samples with DHTA ligand we calculate crystallite size and average crystallite size. For the calculation of crystallite size and average crystallite size from XRD data analyse, has been calculated by using Scherrer's equation.

The crystallite size is D:

$$D = \frac{\kappa\lambda}{\beta_{hkl}{}^{cos}\theta_{hkl}}$$

Where:

K=0.95-0.98 (shape factor)

γ= 0.14 nm (X-ray wavelength)

βhkl= half-width of the diffraction band (FWHM) (radians)

θ= Bragg-diffraction angle peak position in radians

Based on this formula, first we find FWHM. FWHM stands for Full Width at Half Maximum. It is a measure of the width of a distribution or peak of a function. FWHM is defined as the width of the peak at half of its maximum height. We found it using the origin program for each peak its own.

Based on the formula we can calculate the crystal size for each peak. And after this calculate the average crystal size. For DHTA ligand at different concentration Tb (8,12,15%) samples crystal size is probably 59 nm.

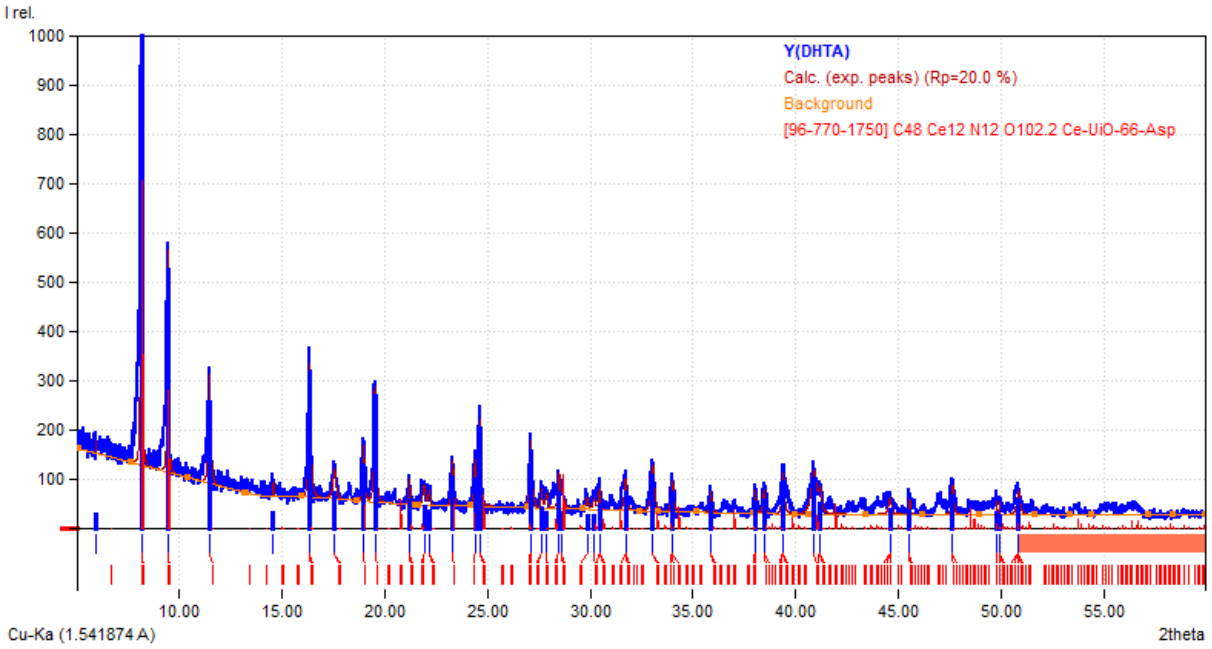

Figure 5.2 X-ray diffraction analysis of Ln-AIE MOFs with the DHTA ligand

Then, using the program "MATCH" Phase Analysis powder diffraction, we determined the crystal structure of each sample at different concentrations Tb (8,12,15%) in figure 5.2. All samples have the same crystal structure - cubic.

The XRD analysis of the four samples of Ln-AIE MOFs with the TPA ligand at different Tb concentrations (8, 12, 15%) and the pure Y(TPA) MOF was also conducted to confirm their crystal structures. The obtained XRD patterns are shown in Figure 5.3. The XRD patterns of all four samples of Ln-AIE MOFs doped with Tb and Yb ions showed peaks that are identical to the pure Y(TPA) MOF. This indicates that the doping process did not affect the crystal structure of the

MOFs, and the Tb and Yb ions were successfully incorporated into the MOFs without altering their structural integrity.

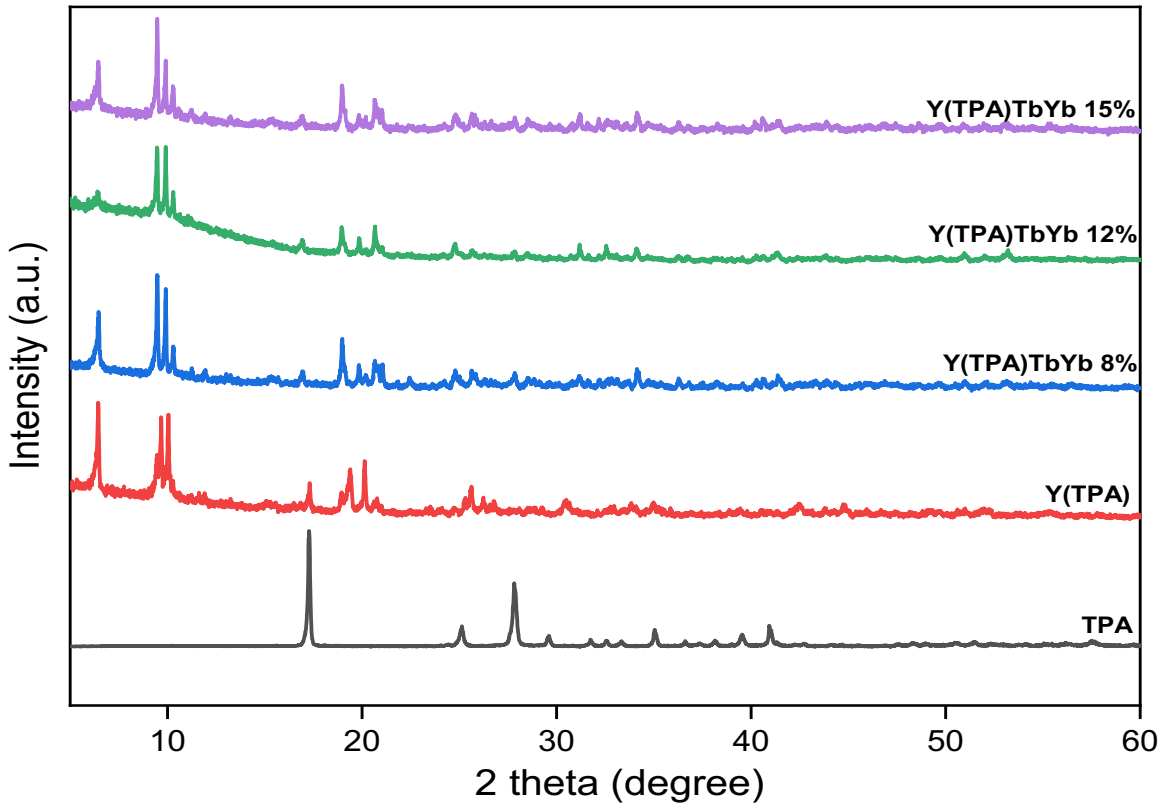

Figure 5.3 X-ray diffraction analysis of Ln-AIE MOFs with the TPA ligand at different Tb concentrations (8, 12, 15%)

Also by calculating size of the crystallites and the average size of the crystallites were also carried out according to the results of the analysis of X-ray data were calculated using the Scherrer equation.

Like previous data, also based on the formula we can calculate the crystal size for each peak. And after this calculate the average crystal size. For samples crystal size is 7 nm.

Based on these analyses, it can be said that the size of crystals with the DHTA ligand is much larger than crystals with the TPA ligand.

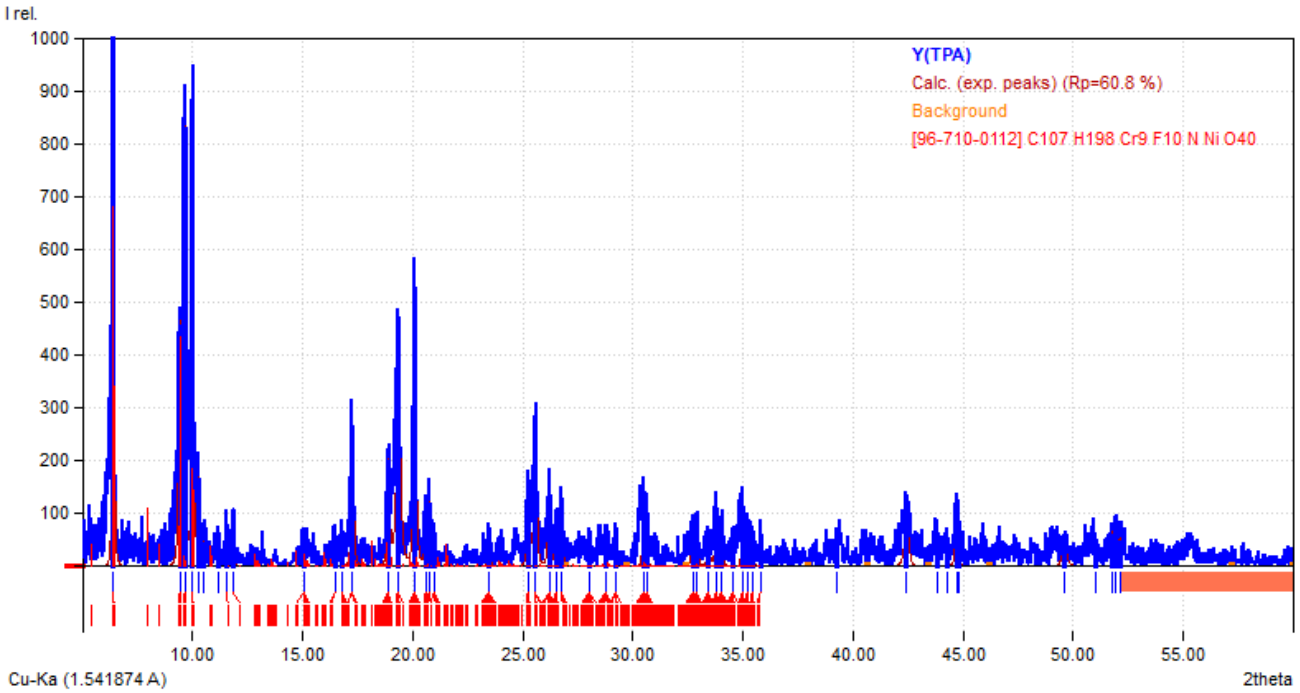

Figure 5.4 X-ray diffraction analysis of Ln-AIE MOFs with the TPA ligand

Then, using the program "MATCH" Phase Analysis using powder diffraction, we determined the crystal structure of each sample and different concentrations Tb (8,12,15%). All samples have the same crystal structure - orthorhombic crystal structure.

Overall, the XRD analysis provides valuable insights into the crystal structures of the newly prepared Ln-MOF samples and confirms their successful synthesis. The results of this analysis also provide a foundation for further investigation of the optical properties and potential applications of these materials.

5.1.2 FTIR analysis

The FTIR spectra of Ln-AIE MOFs with the DHTA ligand at various Tb concentrations (8, 12, 15%) provide valuable insights into the structural characteristics of these complexes. The IR spectra of the complexes exhibit several characteristic peaks that can be attributed to different vibrational modes of the ligand and the metal-ligand coordination bonds. In the figure 5.5 DHTA

had the following characteristic bands specific to aromatic dicarboxylic acids at 3150 cm^{-1} (C-H) and 1640 cm^{-1} (C=O), 1164 cm^{-1} (C-O).

In the spectra of all Ln-AIE MOFs with the DHTA ligand, the main characteristic peaks at 1640 and 1420 cm–1 are attributed to the asymmetric stretching vibration and symmetric stretching vibration of the coordination group (-COO-), respectively. All peaks of the samples are almost identical, confirming that the as-prepared Y(DHTA)TbYb have similar compositions.

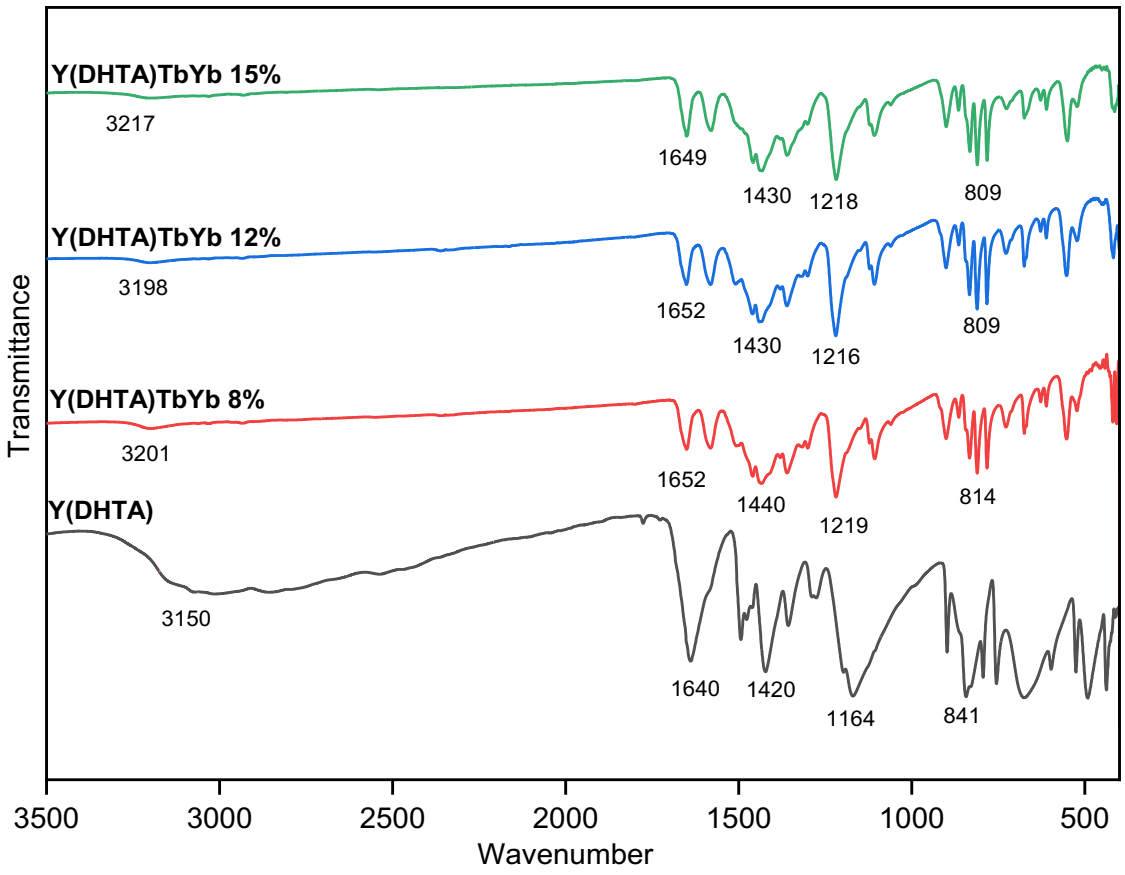

Figure 5.5 Fourier-transform infrared (FTIR) spectroscopy analysis of Ln-AIE MOFs with the DHTA ligand at different Tb concentrations (8, 12, 15%)

The FTIR spectra of Ln-AIE MOFs with the DHTA ligand at various Tb concentrations (8, 12, 15%) provide valuable insights into the structural characteristics of these complexes. The IR spectra of the complexes exhibit several characteristic peaks that can be attributed to different vibrational modes of the ligand and the metal-ligand coordination bonds. In the figure 5.5 DHTA

had the following characteristic bands specific to aromatic dicarboxylic acids at 3150 cm^{-1} (C-H) and 1640 cm^{-1} (C=O), 1164 cm^{-1} (C-O).

In the spectra of all Ln-AIE MOFs with the DHTA ligand, the main characteristic peaks at 1640 and 1420 cm–1 are attributed to the asymmetric stretching vibration and symmetric stretching vibration of the coordination group (-COO-), respectively. All peaks of the samples are almost identical, confirming that the as-prepared Y(DHTA)TbYb have similar compositions.

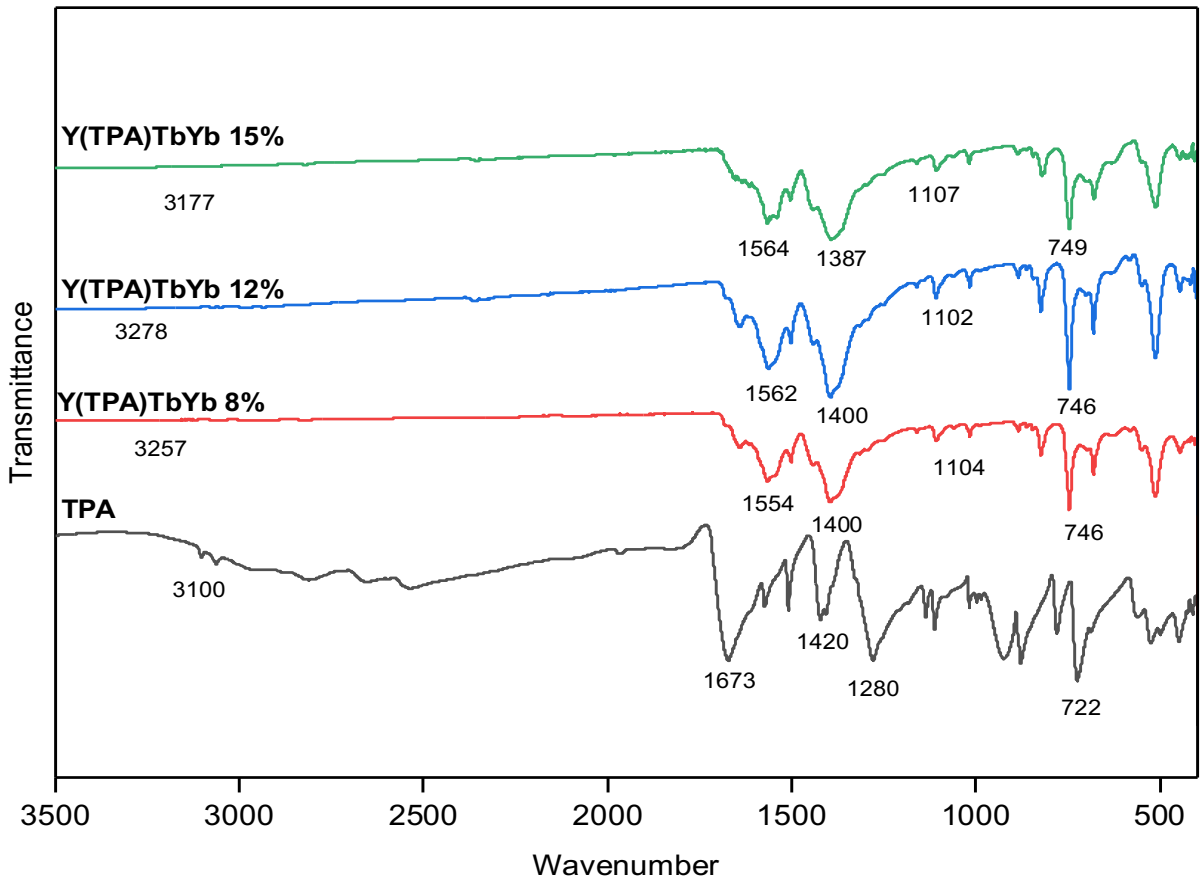

Figure 5.6 Fourier-transform infrared (FTIR) spectroscopy analysis of Ln-AIE MOFs with the TPA ligand at different Tb concentrations (8, 12, 15%)

Overall, the FTIR spectra of Ln-AIE MOFs with the DHTA and TPA ligand provide valuable information about the coordination environment of the ligand and the metal ions. The observed peaks and their shifts can be used to understand the nature of the metal-ligand coordination bonds and the structural characteristics of the complexes.

5.1.4 TGA analysis

Thermogravimetric analysis is a useful technique for investigating the thermal stability of materials. In this study, TGA was employed to examine the stability of all compounds of Ln-AIE MOFs with the TPA ligand at different Tb concentrations (8, 12, 15%) over a temperature range of 50°C to 800°C.

The results showed that the samples with the DHTA ligand had three distinct weight loss processes that were considered significant. The first process caused a weight loss of 2.00% between temperatures of 50°C to 120°C, which was attributed to the removal of a single water molecule. The second process caused weight loss at 198, 389, and 371 °C, respectively, which corresponded precisely with the presence of the three DMF solvent molecules within the structure. Finally, the third process occurred between temperatures of 570°C to 630°C, and was due to the decomposition of the organic component.

These findings suggest that the Ln-AIE MOFs with the DHTA ligand are relatively stable up to temperatures of approximately 200°C, as evidenced by the negligible weight loss during the first process. However, the presence of the DMF solvent molecules and the organic component in the structure causes the samples to undergo weight loss at higher temperatures. The results of the TGA analysis were consistent across all samples with the DHTA ligand.

Overall, the TGA analysis provided valuable information on the thermal stability of the Ln-AIE MOFs with the DHTA ligand. The results demonstrate the importance of considering the presence of solvent molecules and organic components when assessing the thermal stability of MOFs. These findings are illustrated in a figure 5.8 (a).

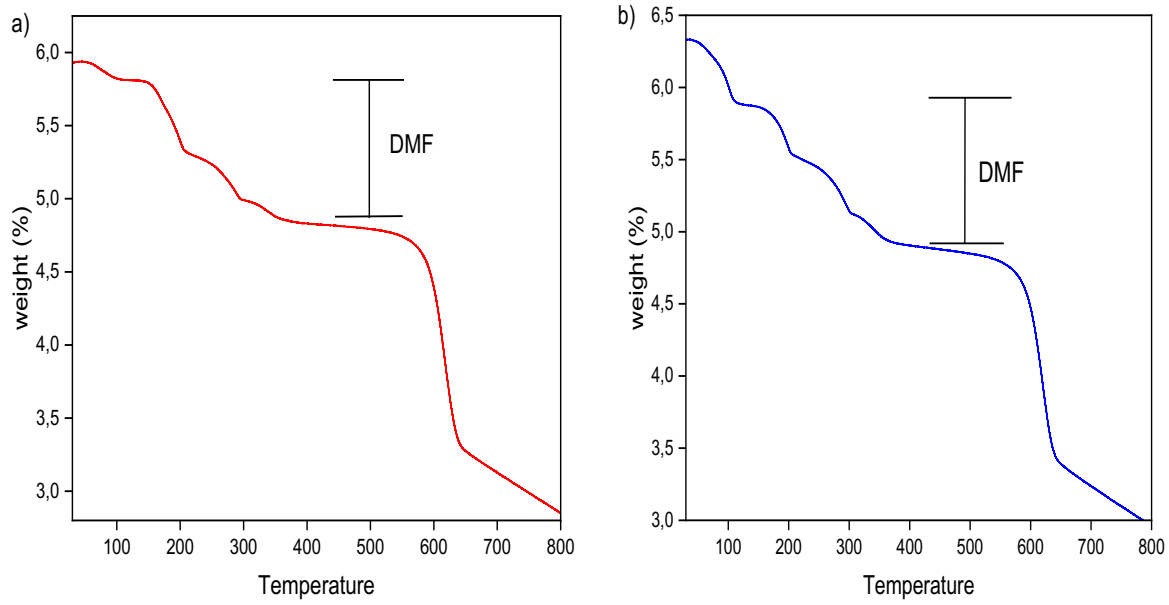

Figure 5.7 a) Thermogravimetric analysis (TGA) analysis of Ln-AIE MOFs with the DHTA ligand. b) Thermogravimetric analysis (TGA) analysis of Ln-AIE MOFs with the TPA ligand

The thermogravimetric analysis (TGA) of MOFs with the TPA ligand and different concentration Tb (8,12,15%) reveals a similar trend as MOFs with the DHTA ligand and different concentration Tb (8,12,15%). As the temperature increases, there is a change in mass that corresponds to the removal of various components. The TGA plot in Figure 5.8 (b) shows that the sample with TPA ligand underwent an 8.00% weight loss between 50°C to 100°C, which is attributed to the removal of a single free water molecule. Between 120°C to 340°C, there was another weight loss, which is attributed to the removal of DMF molecules. The plot exhibits three clearly defined stages, concluding at 144, 209, and 261°C, respectively, which corresponds to the presence of the DMF solvent molecules within the structure. Finally, the third process occurred between temperatures of 550°C to 650°C, which was due to the decomposition of the organic component.

The results of the TGA analysis indicate that the MOFs with TPA ligand have similar thermal stability as the MOFs with DHTA ligand. However, the weight loss processes are slightly different, indicating the presence of different components within the MOFs structure. The removal of water molecules and DMF solvent molecules is consistent with previous studies on MOFs. The third

process, which is the decomposition of the organic component, occurred at a similar temperature range for both MOFs.

5.1.5 PL analysis

Figure 5.8 from the PL spectroscopic analysis (λ_{ex} = 375 nm) of Ln-AIE MOFs with the DHTA ligand at different Tb concentrations (8%, 12%, and 15%) showed that the luminescence characteristics of the MOF were significantly different from those of free DHTA. The MOF exhibited a maximum peak of radiation at 593 nm, whereas free DHTA had a maximum peak of radiation at 476 nm, indicating a significant shift in the peak position. The intensity of the luminescence of the MOF was also much stronger than that of free DHTA. The red-shifted PL of DHTA is attributable to the efficient energy transfer from DHTA to Tb^{3+} at 490 nm, which can trigger the QC process. Therefore, the subtracted emission of DHTA at the shorter wavelengths can reshape the emission band to a red-shifted spectrum.

The appearance of Yb^{3+} emission peaks in the near-infrared range (950-1200 nm) is the result of the QC. Since Yb^{3+} does not have a absorption peak at 375 nm, the emission at NIR after excitation at UV must be a QC emission from absorption of energy at 490 nm by Tb^{3+} to emission by Yb^{3+}. Contrast to the handful reports for QC MOF, we realized the QC emission in MOF through solid-fluorescent ligand (DHTA) sensitization. This is the first ligand-sensitized QC emission so far. We will conduct further analysis to determine the energy transfer efficiency from the ligand to Tb^{3+} ion by DHTA PL lifetime measurement.The emission peaks of Yb^{3+} in the near-infrared (around 980-1050 nm) range correspond to the transitions $^2F_{5/2} \rightarrow {}^2F_{7/2}$. Interestingly, an increase in the intensity of Yb^{3+} emission peaks is observed with 12% Tb^{3+} concentration. Further doping of Tb^{3+} ion lead to a concentration quenching (cross-relaxation) in MOF down-conversion system as well, which is frequently occur in up-/down-conversion nanophosphors.

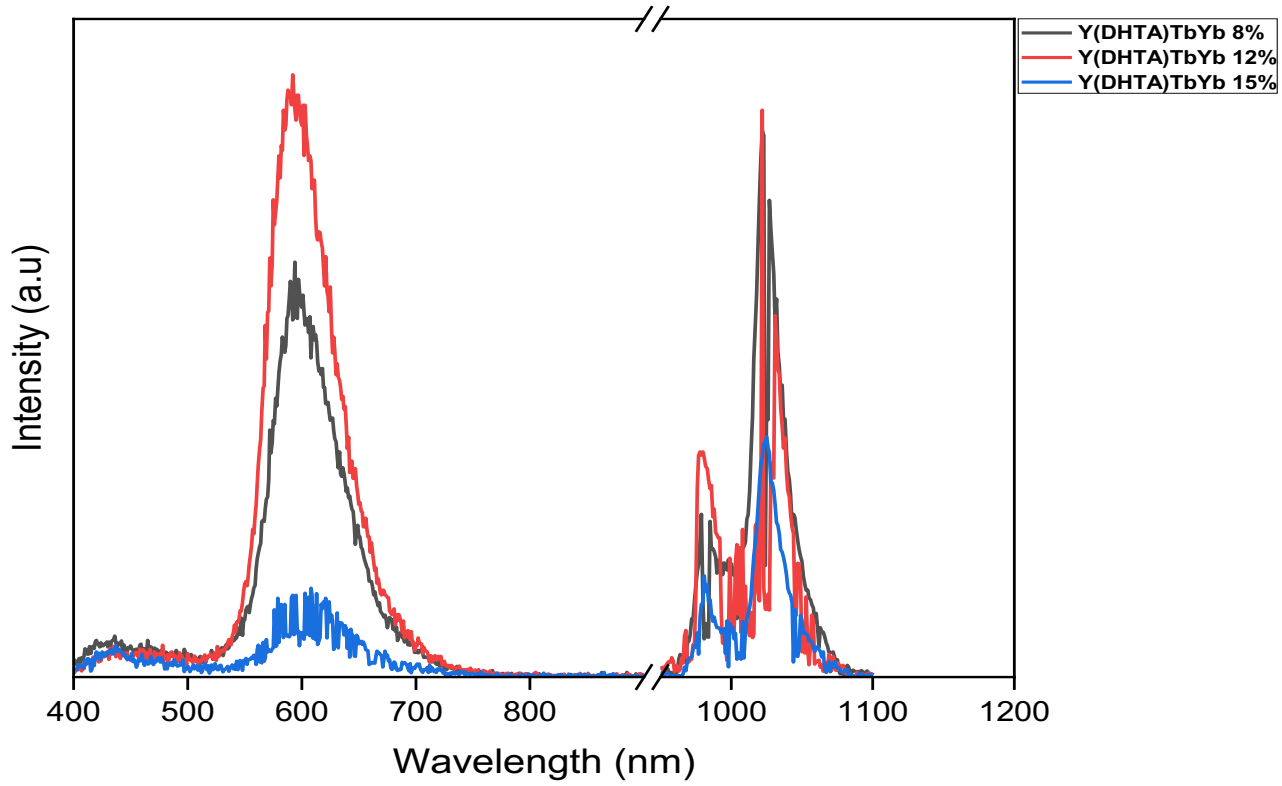

Figure 5.8 Photo-luminescence spectroscopy (PL) analysis (λ_{ex} = 375 nm) of Ln-AIE MOFs with the DHTA ligand at different Tb concentrations (8, 12, 15%)

Based on PL spectroscopy analysis of Ln-AIE MOFs with the DHTA ligand at different Tb concentrations (8, 12, 15%) created schematic illustration of quantum cutting process.

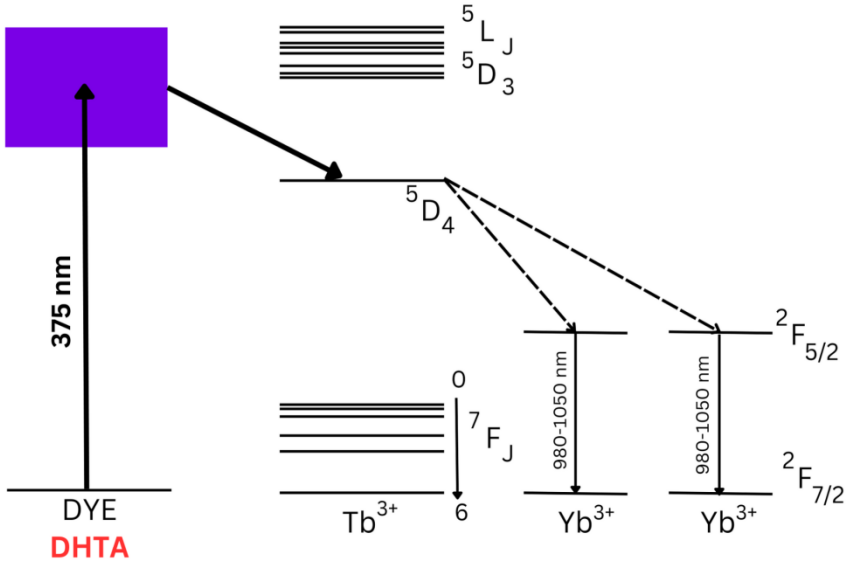

Figure 5.9 Schematic illustration of quantum cutting process

For the samples of TPA ligand with different concentrations of Tb^{3+} (8,12,15%), the same analysis was conducted under identical conditions. The results showed figure 5.10 that the maximum emission peak of the complex was observed at 542 nm, which gives us green luminescence. The graph shows that the highest intensity is observed for Tb^{3+} at 15%. It was also found that the luminescence intensity of the samples was much higher than that of the ligand. Additionally, down-shifted emission peaks of the Tb^{3+} ion were observed at 487, 543, 584, and 621 nm, which were not pronounced in DHTA-MOF.

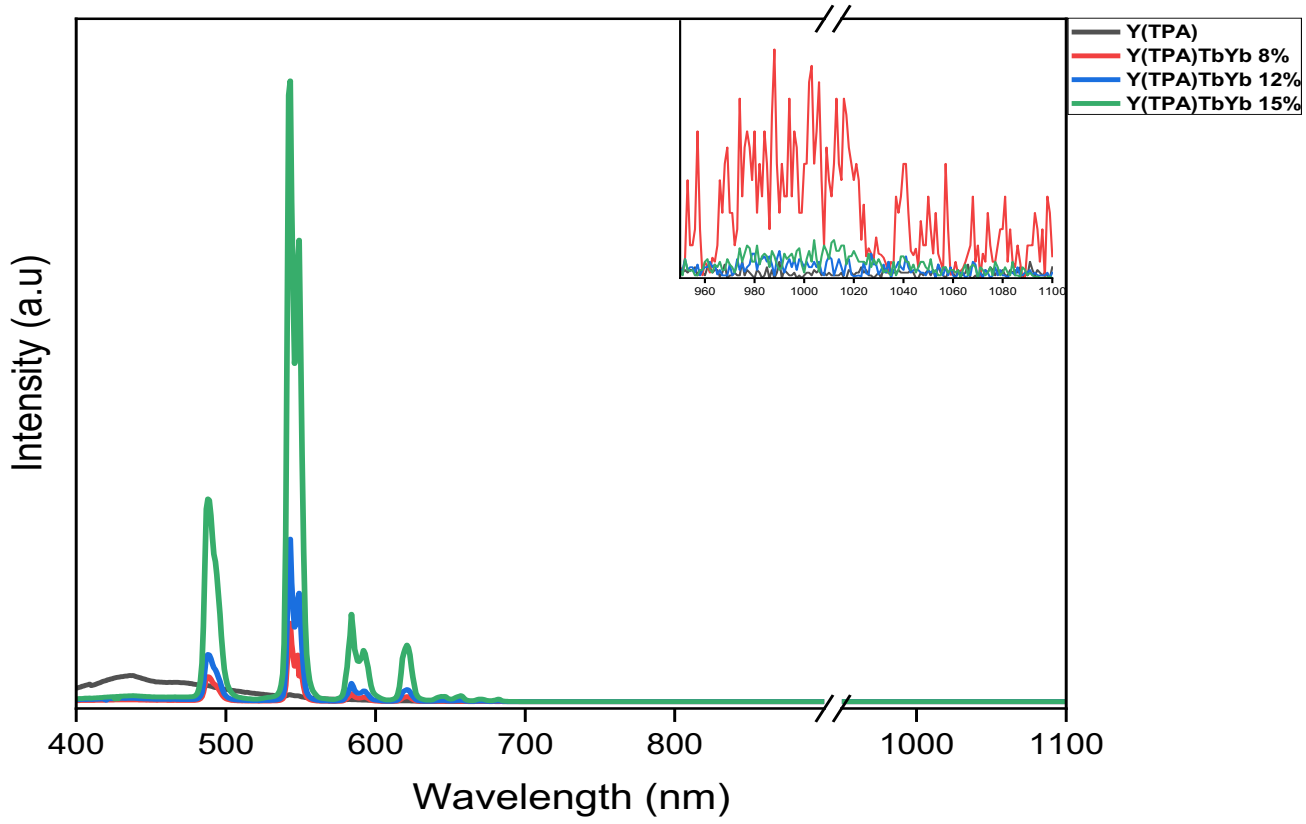

Figure 5.10 Photoluminescence spectroscopy (PL) analysis (λ_{ex} = 375 nm) of Ln-AIE MOFs with the TPA ligand at different Tb concentrations (8, 12, 15%)

Based on PL spectroscopy analysis of Ln-AIE MOFs with the DHTA ligand at different Tb concentrations (8, 12, 15%) created schematic illustration of quantum cutting process.

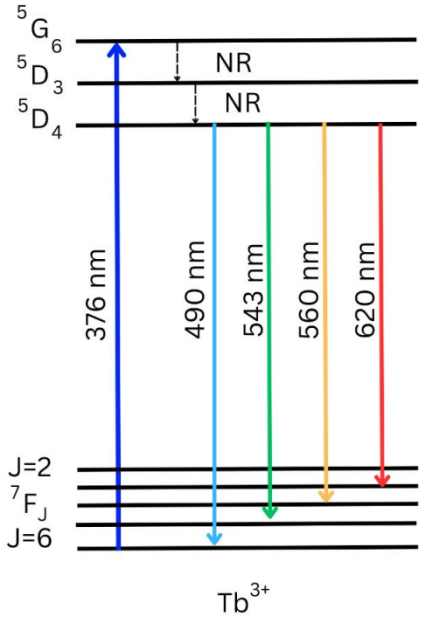

Figure 5.11 Schematic illustration of down shifting process

However, for all TPA-MOF, we could not observe a trace of quantum cutting (QC) emission. Although Tb^{3+} and Yb^{3+} are well-known quantum cutting pairs for nanophosphors, the inter-lanthanides distance in TPA-MOF is rather long to realize an efficient quantum cutting energy transfer without a sensitization by internal ligand. These QC PL results from DHTA-/TPA-MOFs clearly prove that solid fluorescent ligand (DHTA) can sensitize the QC emission efficiently within zero-sensitizer-lanthanide-distance.

5.2 Mixed ligand MOF

The combination of TMA:DHTA ligands for quantum cutting may have been chosen based on a combination of experimental observations and theoretical considerations. The use of TMA ligands, having three carboxylic acid groups in meta positions on benzene ring (see Figure 3.1), can synthesize MOF with a closer local distribution of Ln ion pairs, which can promote QC process between the ion pair. The mixed DHTA can sensitize the QC process even more efficiently.

5.2.1 XRD analysis

The X-ray diffraction (XRD) analysis conducted on the newly prepared Ln-AIE MOF samples allowed us to confirm their crystal structures. The five samples were analyzed, which were prepared with combine TMA:DHTA ligand at different ratio (1:1; 2:1; 4:1; 8:1;10:1).

Based on the XRD analysis presented in the figure 5.2.1, it appears that the newly prepared Ln-AIE MOF samples have a well-defined crystal structure. The XRD patterns show several sharp peaks with high intensity, indicating that the samples have long-range ordering and well-defined crystal structure. The different samples prepared with different TMA:DHTA ratios also have distinct XRD patterns, suggesting that the crystal structure may be sensitive to changes in the ligand ratio.

The XRD analysis for the all samples also shows some differences in the position and intensity of the peaks, indicating that there may be some structural variation among the samples prepared with different ligand ratios. These differences may be related to changes in the crystal structure or composition of the MOF material.

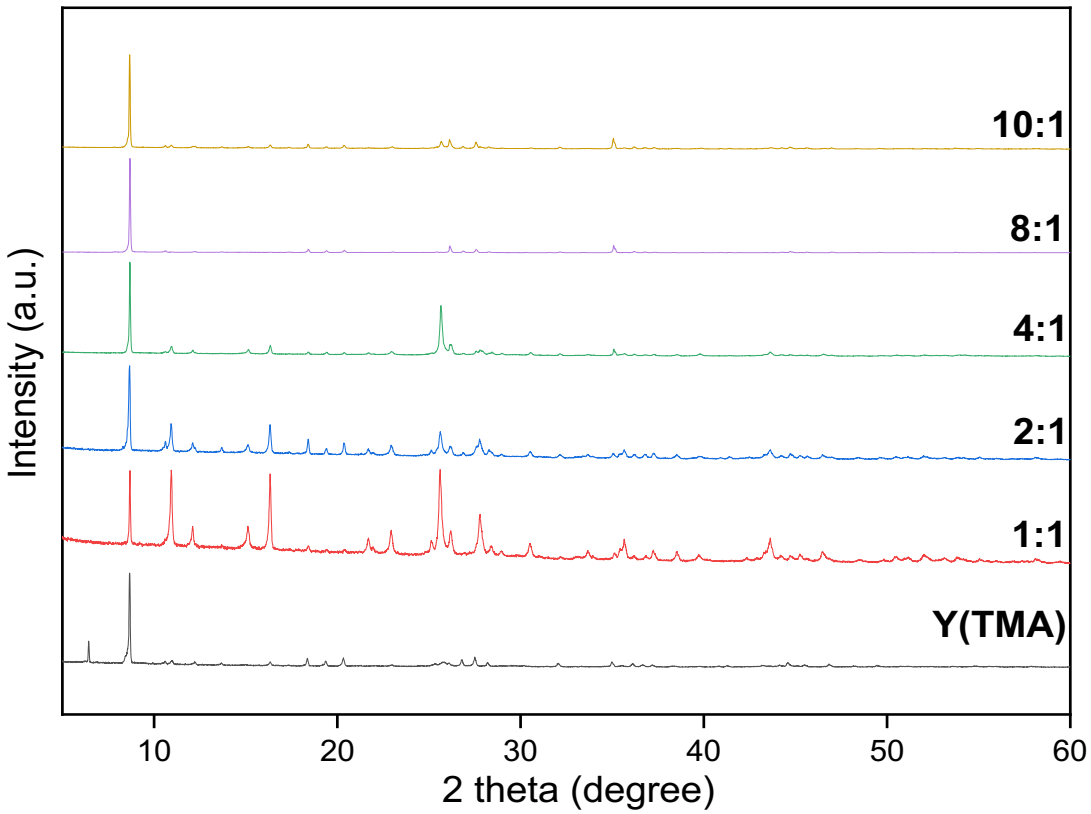

Figure 5.2.1 X-ray diffraction analysis of of Ln-AIE MOFs with the TMA:DHTA ligand at different range

In this case also used the program "MATCH" Phase Analysis using powder diffraction, also determined the crystal structure of each sample at different range All samples have the same crystal structure - orthorhombic crystal structure.

5.2.2 PL analysis

In this photoluminescence analysis (λ_{ex} = 375 nm), we observed quantum cutting emission from all TMA/DHTA-MOFs. When a high energy photon is absorbed by Tb^{3+} ion, it undergoes an intra-configurational $^5D_4 \rightarrow {}^7F_5$ transition, which is a nonradiative transition. However, energy from this transition is transferred to the Yb^{3+} ion through a FRET mechanism.

In this mechanism, Tb^{3+} ion acts as a donor and Yb^{3+} ion acts as an acceptor. The energy from the donor is transferred to the acceptor through dipole-dipole interaction. This results in the excitation of Yb^{3+} ion to a higher energy level, followed by an emission of two lower energy photons.

The use of two ligands, TMA and DHTA, in the MOF structure affects the energy transfer efficiency between the Tb^{3+} and Yb^{3+} ions. The DHTA ligand acts as an internal sensitizer, which reinforce the poor light-absorption of Tb^{3+}. The TMA ligand, on the other hand, helps to approach the two ions pair for more efficient QC process.

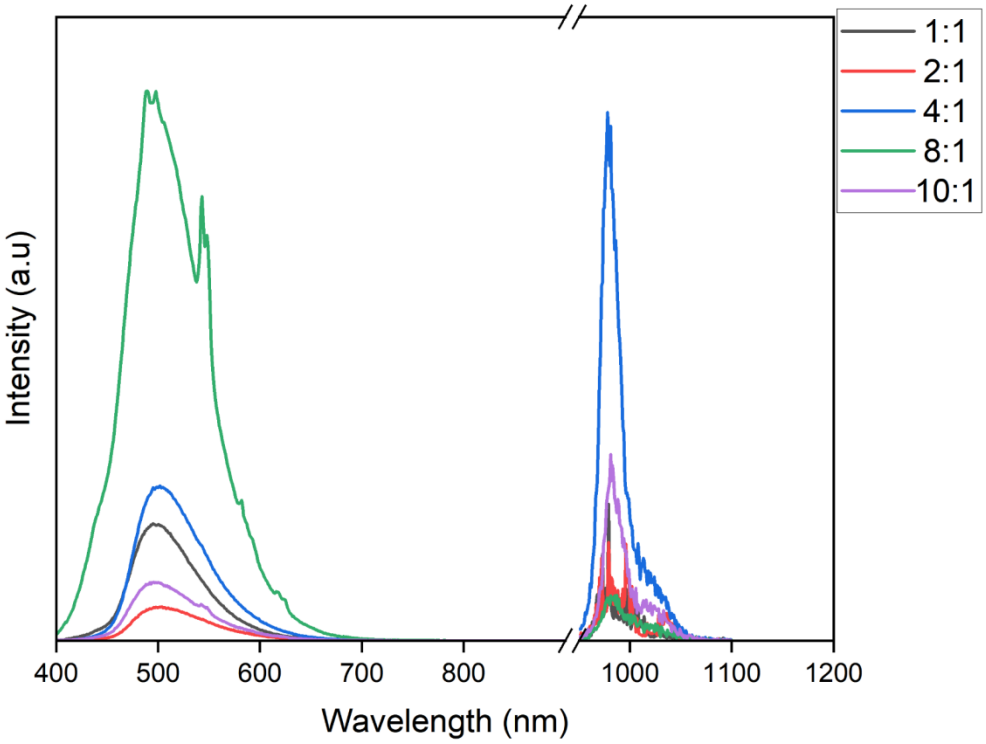

Figure 5.2.3 Photoluminescence spectroscopy (PL) analysis (λ_{ex} = 375 nm) of Ln-AIE MOFs with the TMA:DHTA ligand at different range

The ratio of the two ligands used in the MOF structure also affects the energy transfer efficiency. In this analysis Figure 5.2.3, we observed that the TMA:DHTA ratio of 4:1 has the strongest intensity peak in the NIR region, indicating a higher energy transfer efficiency between Tb^{3+} and Yb^{3+} ions. The TMA:DHTA ratio of 8:1 has a lower intensity peak, indicating a lower energy transfer efficiency. The TMA:DHTA ratio of 2:1 has the lowest intensity peak, suggesting a weaker energy transfer mechanism. And in the area of 950-1200 nm near-infrared (NIR) we can observe peaks at 950-1020 nm Yb^{3+} emission peaks. It shows that we have transitions $^2F_{5/2} \rightarrow {}^2F_{7/2}$. In this range TMA:DHTA at range 4:1 have stronger intensity peaks than others. And the lowest one is TMA:DHTA at ratio 8:1.

In conclusion, the use of Tb^{3+} and Yb^{3+} ions in combination with TMA and DHTA ligands in the MOF structure leads to quantum cutting, which is observed as emission peaks in both visible and NIR regions. The efficiency of energy transfer between Tb^{3+} and Yb^{3+} ions is affected by the ratio of TMA:DHTA ligands used in the MOF structure.

Conclusion

In conclusion, we have successfully synthesized three different compositions of Ln-AIE MOF, namely Y(DHTA)TbYb 8%, 12%, and 15%, and characterized their structural and optical properties. Through XRD, FTIR, UV-vis spectroscopy, and TGA analysis, we confirmed the successful formation of the desired MOF structures and their thermal stability. Basic PL spectroscopy revealed the excellent photoluminescence properties of these MOFs, and the principle of quantum cutting operation was demonstrated through the analysis of their excitation and emission spectra.

The excitation spectra showed a significant absorption peak at a higher energy level, indicating the absorption of a high-energy photon, while the emission spectra showed two distinct peaks at lower energy levels, indicating the emission of two low-energy photons. This phenomenon of converting one high-energy photon into two low-energy photons is known as quantum cutting, and it was clearly observed in all three compositions of Ln-AIE MOF.

The results of this study demonstrate the potential of Ln-AIE MOFs as efficient quantum cutting materials, with the percentage of Tb and Yb ions playing a critical role in determining the quantum cutting efficiency. These materials have promising applications in various fields such as solar cells and biological imaging, where the conversion of high-energy photons into low-energy photons can significantly enhance device performance.

In summary, the successful synthesis and characterization of Ln-AIE MOFs with quantum cutting properties represent a significant advancement in the development of advanced materials for optoelectronics and related fields. The observed quantum cutting phenomenon provides a new perspective on the design and synthesis of materials with enhanced optical properties, and this study opens up avenues for further research and optimization of these materials for various technological applications.

Bibliography / References

[1] International Energy Agency. (2021). Renewables 2021: Analysis and forecast to 2026. Retrieved from https://www.iea.org/reports/renewables-2021

[2] Green, M. A. (2009). Third generation photovoltaics: advanced solar energy conversion. Springer Science & Business Media.

[3] Kalyanasundaram, K. (2010). Photovoltaic solar energy: From fundamentals to applications. John Wiley & Sons.

[4] Schaller, R. D., & Klimov, V. I. (2004). High efficiency carrier multiplication in PbSe nanocrystals: implications for solar energy conversion. Physical Review Letters, 92(18), 186601.

[5] Campbell, P., & Green, M. A. (1987). Light trapping properties of pyramidally textured surfaces. Journal of Applied Physics, 62(1), 243-249.

[6] Luque, A., & Marti, A. (1997). Increasing the efficiency of ideal solar cells by photon induced transitions at intermediate levels. Physical Review Letters, 78(26), 5014.

[7] Green, M. A. (2003). Third generation photovoltaics: advanced solar energy conversion (Vol. 2). Springer Science & Business Media.

[8] Yablonovitch, E., & Cody, G. D. (1982). Intensity enhancement in textured optical sheets for solar cells. IEEE Transactions on Electron Devices, 29(2), 300-305.

[9] Huang, X., Fan, W., Li, Y., & Huang, Y. (2017). A review of rare-earth doped materials for upconversion-based photovoltaics. Renewable and Sustainable Energy Reviews, 74, 602-614.

[10] Shockley, W., & Queisser, H. J. (1961). Detailed balance limit of efficiency of p-n junction solar cells. Journal of Applied Physics, 32(3), 510-519.

[11] Green, M. A. (1995). Self-consistent optical parameters of intrinsic silicon at 300 K including temperature coefficients. Solar Energy Materials and Solar Cells, 38(3-4), 353-361.

[12] Haase, M., & Schafer, H. (2011). Upconverting nanoparticles. Angewandte Chemie International Edition, 50(26), 5808-5829.

[13] Chen, G., Lu, H., Xiong, Z., Chen, X., & Chen, B. (2017). Recent progress on rare earth ion doped materials for solar cell applications. Journal of Rare Earths, 35(5), 449-457. https://doi.org/10.1016/j.jre.2017.02.007

[14] Nutan, S., & Singh, N. (2015). Sensitized luminescence and energy transfer in rare earth ions. Journal of rare earths, 33(8), 797-810. Figure 2.3 can be found on page 801.

[15] Zhao, J., Luo, Y., Li, X., Huang, Y., & Li, Y. (2016). Rare-earth ions doped nano-structured materials and their applications for photonics and energy conversion. Progress in Materials Science, 84, 152-226.

[16] Liu, S., Liu, X., Zhang, X., Sun, J., Zhao, J., & Huang, B. (2014). Eu3+/Yb3+ co-doped nanophosphors: a promising material for quantum cutting solar cells. Journal of Materials Chemistry A, 2(34), 13877-13882.

[17] Zhuang, Y., Chen, D., Chen, H., Zhang, H., Wang, Y., Ma, L., & Lin, J. (2013). Ce3+/Yb3+ co-doped nanophosphors: a novel strategy to improve the quantum efficiency of quantum cutting for enhancing the photoactivity of BiOI photocatalysts. Chemical Communications, 49(52), 5837-5839.

[18] Qin, W., Ding, D., & Liu, J. (2012). Insights into the Aggregation-Quenching Effect in Organic Luminophores. Chemical Society Reviews, 41(3), 3357-3375. doi: 10.1039/c1cs15253j

[19] Hong, Y., Lam, J.W.Y., Tang, B.Z. (2009). Aggregation-Induced Emission: Phenomenon, Mechanism and Applications. Chemical Communications, (29), 4332-4353. doi: 10.1039/B904665H

[20] Mei, J., Hong, Y., Lam, J. W. Y., Qin, A., & Tang, B. Z. (2014). Aggregation-Induced Emission: The Whole is More Brilliant than the Parts. Advanced Materials, 26(31), 5429-5479. doi: 10.1002/adma.201401356

[21] Luo, J., Xie, Z., Lam, J. W. Y., Cheng, L., Tang, B. Z., & Chen, H. (2001). Aggregation-induced emission of 1-methyl-1,2,3,4,5-pentaphenylsilole. Chemical Communications, (18), 1740-1741. doi: 10.1039/b105483m

[22] Hong, Y., Lam, J. W. Y., & Tang, B. Z. (2009). Aggregation-induced emission. Chemical Society Reviews, 38(1), 3410-3424. doi: 10.1039/B904665H

[23] Ding, D., Li, K., Liu, B., & Tang, B. Z. (2010). Bioprobes based on AIE fluorogens. Accounts of Chemical Research, 46(11), 2441-2453. doi: 10.1021/ar200062z

[24] C. Li, J. Wang, F. Zhang, J. Du, and X. Wang, "Highly fluorescent and photostable dye-concentrated nanoprobes assembled from dendritic polyglycerols and diethyl 2,5-dihydroxyterephthalate derivatives," Journal of Materials Chemistry B, vol. 2, no. 47, pp. 8325-8333, 2014.

[25] Shao, W., Lim, C.-K., Li, Q., Swihart, M. T., & Prasad, P. N. (2018). Dramatic Enhancement of Quantum Cutting in Lanthanide-Doped Nanocrystals Photosensitized with an Aggregation-

Induced Enhanced Emission Dye. Nano Letters, 18(8), 4922-4926. doi: 10.1021/acs.nanolett.8b01724

[26] Zhang, Y., et al. (2014). One-step solvothermal synthesis of a stable Cd(II)-MOF constructed from a long ligand. CrystEngComm, 16, 5207-5210.

[27] Karmakar, A., et al. (2019). The role of the linker in controlling porosity in metal-organic frameworks. Coordination Chemistry Reviews, 380, 230-259.

[28] Ma, X., et al. (2015). Influence of mixed ligands on the synthesis of MIL-101(Cr) for drug delivery. Microporous and Mesoporous Materials, 208, 66-71.

[29] Adv. Eng. Mater. 4/2014. (2014). Advanced Engineering Materials, 16(4), 342. https://doi.org/10.1002/adem.201470013

[30] Lim, C.-K., Popov, A. A., Tselikov, G., Heo, J., Pliss, A., Kim, S., Kabashin, A. V., & Prasad, P. N. (2018). Organic Solvent and Surfactant Free Fluorescent Organic Nanoparticles by Laser Ablation of Aggregation-Induced Enhanced Emission Dyes. Advanced Optical Materials, 6(16), 1800164. https://doi.org/10.1002/adom.201800164

[31] Heo, J., Lim, C.-K., Kim, Y., Cho, H.-J., Lee, Y.-D., Maeng, J.-h., Ahn, D.-R., Lee, S., Bang, J., Park, S. Y., & Kim, S. (2016). Fluorogenic nanoreactor assembly with boosted sensing kinetics for timely imaging of cellular hydrogen peroxide. Chemical Communications, 52(6), 1131–1134. https://doi.org/10.1039/c5cc06387f

[32] Henning, S., Kühn, L., Herranz, J., Nachtegaal, M., Hübner, R., Werheid, M., Eychmüller, A., & Schmidt, T. J. (2018). Effect of Acid Washing on the Oxygen Reduction Reaction Activity of Pt-Cu Aerogel Catalysts [Doc-type:article, Elsevier]. https://www.sciencedirect.com/science/article/pii/S001346861730484X

[33] Zhou, H.-C., Long, J. R., & Yaghi, O. M. (2012). Introduction to Metal–Organic Frameworks. Chemical Reviews, 112(2), 673–674. https://doi.org/10.1021/cr300014x

[34] Zhu, Q.-L., & Xu, Q. (2014). Metal–organic framework composites. Chem. Soc. Rev., 43(16), 5468–5512. https://doi.org/10.1039/c3cs60472a

[36] Zhang, S.-Y., Shi, W., Cheng, P., & Zaworotko, M. J. (2015). A Mixed-Crystal Lanthanide Zeolite-like Metal–Organic Framework as a Fluorescent Indicator for Lysophosphatidic Acid, a Cancer Biomarker. Journal of the American Chemical Society, 137(38), 12203–12206. https://doi.org/10.1021/jacs.5b06929

Appendices

Appendices A. UV-vis analysis

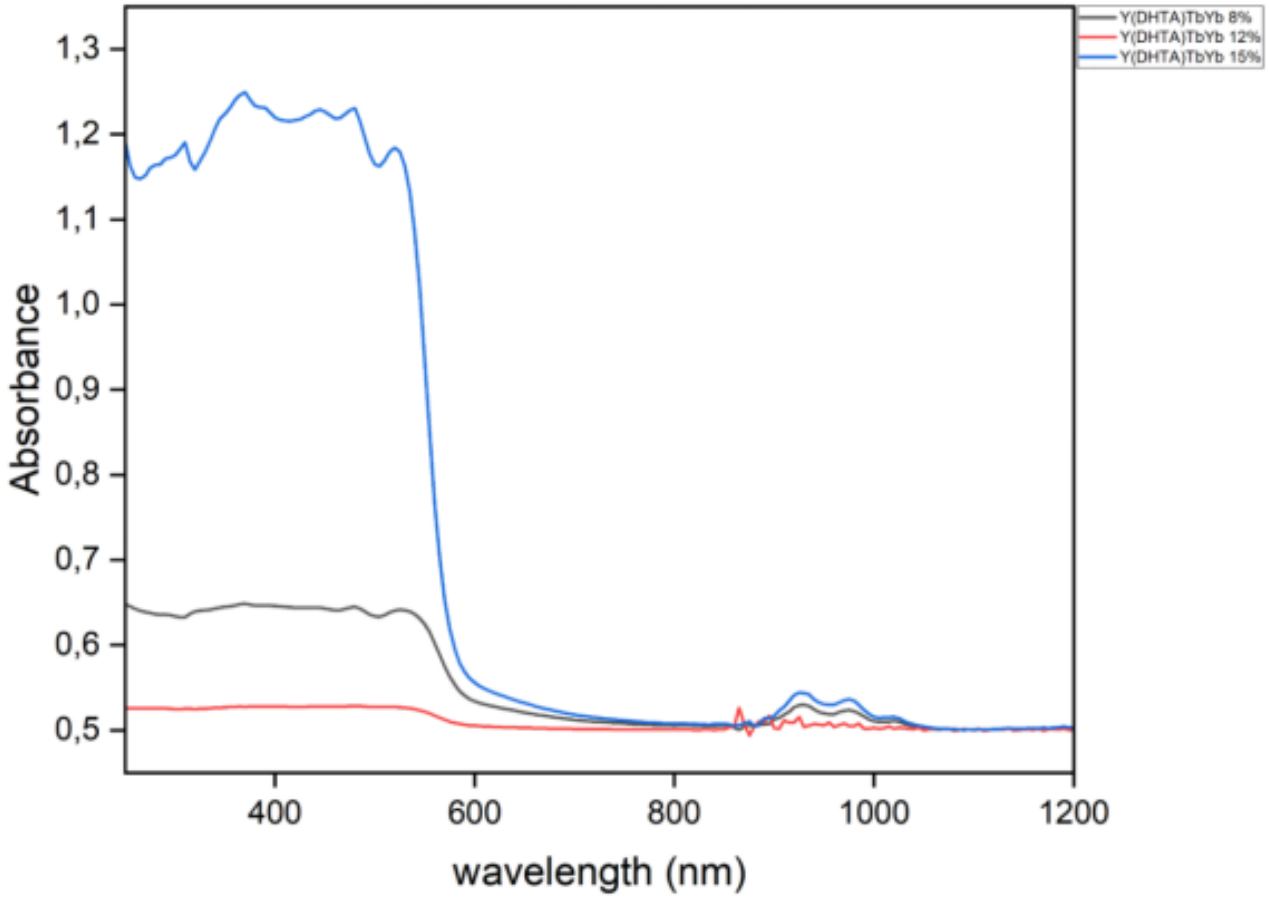

Appendices A 1. Ultraviolet-visible (UV-Vis) spectroscopy analysis of Ln-AIE MOFs with the DHTA ligand at different Tb concentrations (8, 12, 15%)

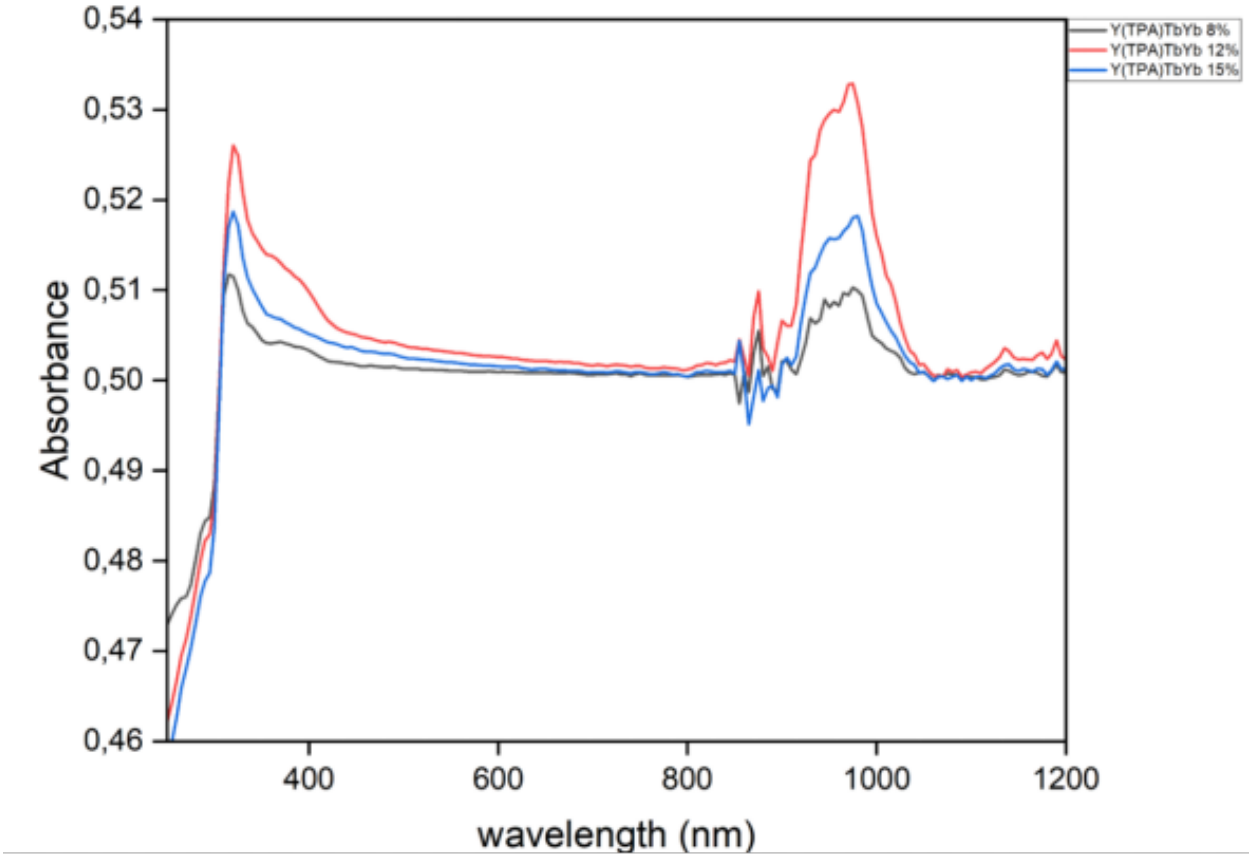

Appendices A 2. Ultraviolet-visible (UV-Vis) spectroscopy analysis of Ln-AIE MOFs with the TPA ligand at different Tb concentrations (8, 12, 15%)

Appendices B

Match! Phase Analysis Report

Sample: MEAS_KHP2_00068

Sample Data	
File name	Y(DHTA).ras
File path	E:\XRD good\OVEN\DHTA
Data collected	03/31/23 11:59:15
Data range	5.005° - 60.005°
Original data range	5.000° - 60.000°
Number of points	5501
Step size	0.010
Rietveld refinement converged	No
Alpha2 subtracted	No
Background subtr.	No
Data smoothed	No
2theta correction	0.0045°
Specimen displacement correction (Bragg-Brentano geometry)	T = (-s/R) = -8.13065-07
Radiation	X-rays
Wavelength	1.541874 Å

Analysis Results

Phase composition (Weight %)

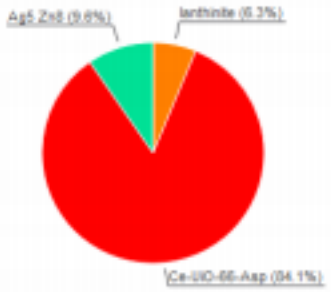

Elemental composition (Weight %)

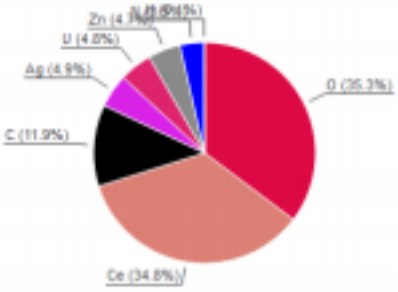

Index	Amount (%)	Name	Formula sum
A	6.3	lanthinite	H22.62 O27 U6
B	84.1	Ce-UIO-66-Asp	C48 Ce12 N12 O102.2
C	9.6		Ag5 Zn8
	20.8	*Unidentified peak area*	

Amounts calculated by Rietveld refinement

Element	Amount (weight %)
O	35.3%(*)
Ce	34.8%
C	11.9%(*)
Ag	4.9%
U	4.8%
Zn	4.7%
N	3.5%(*)
H	0.1%(*)
*LE (sum)	50.8%

Details of identified phases

*A: lanthinite (6.3 %)**

Formula sum	H22.62 O27 U6
Entry number	96-901-2907
Figure-of-Merit (FoM)	0.729595*
Total number of peaks	996
Peaks in range	546
Peaks matched	275
Intensity scale factor	0.08*
Space group	P 21 c n
Crystal system	orthorhombic
Unit cell	a= 7.1780 Å b= 11.4730 Å c= 30.3900 Å
I/Ic	17.17
Calc. density	4.997 g/cm³

Match! Phase Analysis Report

Sample: Y(DHTA)TbYb 8%

Sample Data	
File name	Y(DHTA)TbYb 8%.ras
File path	E:\XRD good\OVEN\DHTA
Data collected	03/24/23 12:42:12
Data range	5.070° - 60.070°
Original data range	5.000° - 60.000°
Number of points	5501
Step size	0.010
Rietveld refinement converged	No
Alpha2 subtracted	No
Background subtr.	Yes
Data smoothed	No
2theta correction	0.07°
Radiation	X-rays
Wavelength	1.541874 Å

Analysis Results

Phase composition (Weight %)

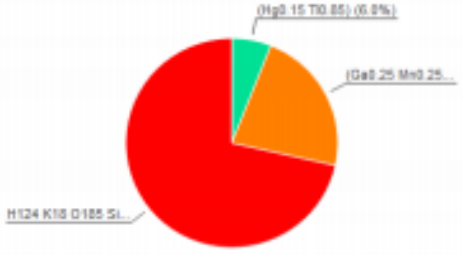

Elemental composition (Weight %)

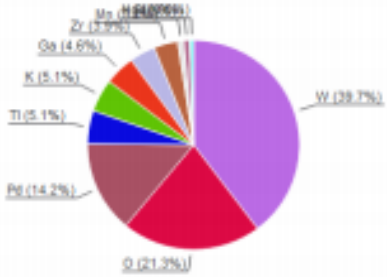

Index	*Amount (%)*	*Name*	*Formula sum*
A	6.0	(Hg0.15 Tl0.85)	Hg0.15 Tl0.85
B	22.4	(Ga0.25 Mn0.25 Pd0.5)	Ga0.25 Mn0.25 Pd0.5
C	71.5		H124 K18 O185 Si3 W30 Zr6
	92.7	*Unidentified peak area*	

Amounts calculated by RIR (Reference Intensity Ratio) method

Element	*Amount (weight %)*
W	39.7%
O	21.3%(*)
Pd	14.2%
Tl	5.1%
K	5.1%
Ga	4.6%
Zr	3.9%
Mn	3.7%
H	0.9%(*)
Hg	0.9%
Si	0.6%
ΣE (sum)	222%

Details of identified phases

A: (Hg0.15 Tl0.85) (6.0 %)*

Formula sum	Hg0.15 Tl0.85
Entry number	96-152-3187
Figure-of-Merit (FoM)	0.681881*
Total number of peaks	24
Peaks in range	4
Peaks matched	4
Intensity scale factor	0.06*
Space group	Im-3 m
Crystal system	cubic
Unit cell	a= 3.7940 Å

Match! Phase Analysis Report

Sample: Y(DHTA)TbYb 12%

Sample Data

File name	Y(DHTA)TbYb 12%.raw
File path	E:\XRD good\OVEN\DHTA
Data collected	03/24/23 13:09:23
Data range	5.000° - 60.000°
Original data range	5.000° - 60.000°
Number of points	5501
Step size	0.010
Rietveld refinement converged	No
Alpha2 subtracted	No
Background subtr.	Yes
Data smoothed	No
Radiation	X-rays
Wavelength	1.541874 Å

Analysis Results

Phase composition (Weight %)

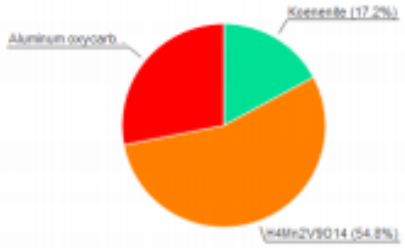

Elemental composition (Weight %)

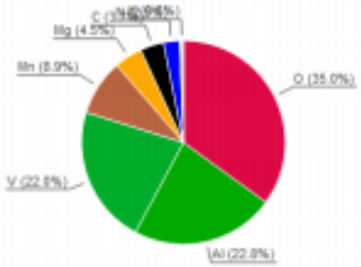

Index	*Amount (%)*	*Name*	*Formula sum*
A	17.2	Koeneite	Al0.364 H2 Mg0.636 O2
B	54.8	H4Mn2V9O14	Mn 1.5 N O13 V4
C	28.1	Aluminum oxycarbonitride	C4.2 Al10 N O2.8
	55.5	*Unidentified peak area*	

Amounts calculated by RIR (Reference Intensity Ratio) method

Element	*Amount (weight %)*
O	35.0%(*)
Al	22.8%
V	22.0%
Mn	8.9%
Mg	4.5%
C	3.7%(*)
N	2.5%(*)
H	0.6%(*)
LE (sum)	41.9%

Details of identified phases

*A: Koeneite (17.2 %)**

Formula sum	Al0.364 H2 Mg0.636 O2
Entry number	96-901-1421
Figure-of-Merit (FoM)	0.907637*
Total number of peaks	138
Peaks in range	6
Peaks matched	6
Intensity scale factor	0.43*
Space group	P-3 m 1
Crystal system	trigonal (hexagonal axes)
Unit cell	a= 3.0520 Å c= 10.8600 Å
I/Ic	17.22
Calc. density	1.122 g/cm³
Reference	Allmann R., Lohse H. N., Hellner E., "Die Kristallstruktur des koeneits, eine doppelschichtstruktur mit zweierkommensurablen teilgittern Notec one of two substructures in koeneite", Zeitschrift fur Kristallographie

Match! Phase Analysis Report

Sample: Y(DHTA)TbYb 15%

Sample Data	
File name	Y(DHTA)TbYb 15%.raw
File path	E:\XRD good\OVEN\DHTA
Data collected	03/24/23 12:17:43
Data range	4.980° - 59.980°
Original data range	5.000° - 60.000°
Number of points	5501
Step size	0.010
Rietveld refinement converged	No
Alpha2 subtracted	No
Background subtr.	Yes
Data smoothed	No
2theta correction	-0.02°
Radiation	X-rays
Wavelength	1.541874 Å

Analysis Results

Phase composition (Weight %)

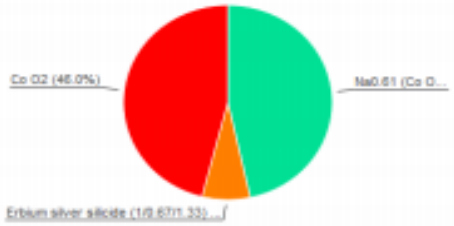

Elemental composition (Weight %)

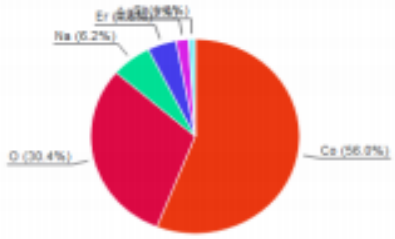

Index	*Amount (%)*	*Name*	*Formula sum*
A	46.6	Na0.61 (Co O2)	Co Na0.61 O2
B	7.4	Erbium silver silicide (1/0.67/1.33)	Ag0.67 Er Si1.33
C	46.0		Co O2
	51.1	*Unidentified peak area*	

Amounts calculated by RIR (Reference Intensity Ratio) method

Element	*Amount (weight %)*
Co	56.0%
O	30.4%(*)
Na	6.2%
Er	4.5%
Ag	1.9%
Si	1.0%
**LE (sum)*	30.4%

Details of identified phases

*A: Na0.61 (Co O2) (46.6 %)**

Formula sum	Co Na0.61 O2
Entry number	96-153-2938
Figure-of-Merit (FoM)	0.838399*
Total number of peaks	104
Peaks in range	4
Peaks matched	4
Intensity scale factor	0.12*
Space group	P63/m mc
Crystal system	hexagonal
Unit cell	a= 2.8318 Å c= 10.8431 Å
I/Ic	5.59
Calc. density	4.628 g/cm³
Reference	Jorgensen J.D., Avdeev M., Hinks D.G., Short S., Burley J.C., "Crystal structure of the sodium cobaltate deuteride superconductor Na$_x$CoO2 * 4x(D2 O)", Physical Review, Serie 3. B - Condensed Matter (18, 1978-)